[46] Flesch M, Hoper A, Dell'Italia L, Evans K, Bond R, Peshock R, et al. Activation and functional significance of the renin-angiotensin system in mice with cardiac restricted overexpression of tumor necrosis factor. Circulation 2003;108:598-604.

[47] Ron D, Brasier AR, Habener JF. Transcriptional regulation of hepatic angiotensinogen gene expression by the acute-phase response. Mol Cell Endocrinol 1990;74:C97-C104.

[48] Hotamisligil GS, Arner P, Caro JF, Atkinson RL, Spiegelman BM. Increased adipose tissue expression of tumor necrosis factor–alpha in human obesity and insulin resistance. J Clin Invest 1995;95: 2409-15.

[49] Xu H, Barnes GT, Yang Q, Tan G, Yang D, Chou CJ, et al. Chronic inflammation in fat plays a crucial role in the development of obesity-related insulin resistance. J Clin Invest 2003;112:1821-30.

[50] Ron D, Brasier AR, McGehee Jr RE, Habener JF. Tumor necrosis factor–induced reversal of adipocytic phenotype of 3T3-L1 cells is preceded by a loss of nuclear CCAAT/enhancer binding protein (C/EBP). J Clin Invest 1992;89:223-33.

Glucocorticoid reamplification within cells intensifies NF-κB and MAPK signaling and reinforces inflammation in activated preadipocytes

Takako Ishii-Yonemoto, Hiroaki Masuzaki, Shintaro Yasue, Sadanori Okada, Chisayo Kozuka, Tomohiro Tanaka, Michio Noguchi, Tsutomu Tomita, Junji Fujikura, Yuji Yamamoto, Ken Ebihara, Kiminori Hosoda, and Kazuwa Nakao

Division of Endocrinology and Metabolism, Department of Medicine and Clinical Science, Kyoto University Graduate School of Medicine, Sakyoku, Japan

Ishii-Yonemoto T, Masuzaki H, Yasue S, Okada S, Kozuka C, Tanaka T, Noguchi M, Tomita T, Fujikura J, Yamamoto Y, Ebihara K, Hosoda K, Nakao K. Glucocorticoid reamplification within cells intensifies NF-κB and MAPK signaling and reinforces inflammation in activated preadipocytes. *Am J Physiol Endocrinol Metab* 298: E930–E940, 2010. First published September 23, 2009; doi:10.1152/ajpendo.00320.2009.—Increased expression and activity of the intracellular glucocorticoid-reactivating enzyme 11β-hydroxysteroid dehydrogenase type 1 (11β-HSD1) contribute to dysfunction of adipose tissue. Although the pathophysiological role of 11β-HSD1 in mature adipocytes has long been investigated, its potential role in preadipocytes still remains obscure. The present study demonstrates that the expression of 11β-HSD1 in preadipocyte-rich stromal vascular fraction (SVF) cells in fat depots from *ob/ob* and diet-induced obese mice was markedly elevated compared with lean control. In 3T3-L1 preadipocytes, the level of mRNA and reductase activity of 11β-HSD1 was augmented by TNF-α, IL-1β, and LPS, with a concomitant increase in inducible nitric oxide synthase (iNOS), monocyte chemoattractant protein-1 (MCP-1), or IL-6 secretion. Pharmacological inhibition of 11β-HSD1 and RNA interference against 11β-HSD1 reduced the mRNA and protein levels of iNOS, MCP-1, and IL-6. In contrast, overexpression of 11β-HSD1 further augmented TNF-α-induced iNOS, IL-6, and MCP-1 expression. Moreover, 11β-HSD1 inhibitors attenuated TNF-α-induced phosphorylation of NF-κB p65 and p38-, JNK-, and ERK1/2-MAPK. Collectively, the present study provides novel evidence that inflammatory stimuli-induced 11β-HSD1 in activated preadipocytes intensifies NF-κB and MAPK signaling pathways and results in further induction of proinflammatory molecules. Not limited to 3T3-L1 preadipocytes, we also demonstrated that the notion was reproducible in the primary SVF cells from obese mice. These findings highlight an unexpected, proinflammatory role of reamplified glucocorticoids within preadipocytes in obese adipose tissue.

11β-hydroxysteroid dehydrogenase type 1; preadipocyte; nuclear factor-κB; mitogen-activated protein kinase; adipose inflammation

OBESE ADIPOSE TISSUE IS CHARACTERIZED by low-grade, chronic inflammation (24, 58). In humans and rodents, it has been shown that intracellular glucocorticoid reactivation is exaggerated in obese adipose tissue (38). Two isoenzymes, 11β-hydroxysteroid dehydrogenase type 1 (11β-HSD1) and type 2 (11β-HSD2), catalyze interconversion between hormonally active cortisol and inactive cortisone (2). In particular, 11β-HSD1 is abundantly expressed in adipose tissue and preferen-

tially reactivates cortisol from cortisone (2). In contrast, 11β-HSD2 inactivates cortisol mainly in tissues involved in water and electrolyte metabolism (60). Transgenic mice overexpressing 11β-HSD1 in adipose tissue display a cluster of fuel dyshomeostasis (61). Conversely, systemic 11β-HSD1 knockouts and adipose-specific 11β-HSD2 overexpressors, which mimic adipose-specific 11β-HSD1 knockouts, are completely protected against diabetes and dyslipidemia on a high-fat diet (14, 30, 31, 42). Interestingly, 11β-HSD1 knockout mice on a high-fat diet showed preferential accumulation of subcutaneous adipose tissue, whereas wild-type mice accumulated considerable fat pads also in visceral (mesenteric) adipose tissue (39). These findings suggest that increased activity of 11β-HSD1 in adipose tissue contributes to dysfunction of adipose tissue and subsequent metabolic derangement.

Adipose tissue is composed of mature adipocytes (~50–70% of total cells), preadipocytes (~20–40%), macrophages (~1–30%), and other cell types (22). Biopsy studies of human adipose tissue demonstrated that the distribution of adipocyte diameter is bimodal, consisting of populations of very small adipocytes ("differentiating preadipocytes") and mature adipocytes (28, 35). Interestingly, the proportion of very small adipocytes was higher in obese people compared with the lean controls (28). Notably, insulin resistance was associated with an expanded population of small adipocytes and decreased expression of differentiation marker genes, suggesting that impairment of adipocyte differentiation may contribute to obesity-associated insulin resistance (35). In this context, a potential link between preadipocyte function and pathophysiology of obese adipose tissue has recently attracted research interest (53, 57).

Many of the genes overexpressed in mature adipocytes are associated with metabolic and secretory function, whereas the most representative function of the genes overexpressed in nonmature adipocytes, i.e., stromal vascular fraction (SVF) cells, is related to inflammation and immune response (9). Macrophage infiltration into obese adipose tissue contributes to local and systemic inflammation in subjects with obesity (63, 65). Furthermore, recent research (12, 48) highlights a pathophysiological role of preadipocytes in obese adipose tissue. In the proinflammatory milieu, preadipocytes act as macrophages (11, 13), share in phagocytic activities (11), and secrete an array of inflammatory substances (13).

A pharmacological dose of glucocorticoids is widely used for anti-inflammatory therapies in human clinics (49). On the other hand, recent research is highlighting the stimulatory effects of glucocorticoids on inflammatory response. Such effects are observed at lower concentrations relevant to phys-

iological stress in vivo (35, 55, 66). Therefore, the potential role of 11β-HSD1 in a variety of inflammatory responses has stimulated academic interest (10, 26). Furthermore, it is known that mature adipocytes abundantly express 11β-HSD1, which is related to adipocyte dysfunction in obese adipose tissue (44, 61). On the other hand, the role of 11β-HSD1 in SVF cells remains largely unclear.

In this context, the present study was designed to explore the expression, regulation, and pathophysiological role of 11β-HSD1 in activated preadipocytes. The results demonstrate that inflammatory stimuli-induced 11β-HSD1 reinforces NF-κB and MAPK signals and results in induction of proinflammatory molecules.

MATERIALS AND METHODS

Reagents and chemicals. All reagents were of analytical grade unless otherwise indicated. TNF-α, IL-1β, LPS, and carbenoxolone (3, 52), a nonselective inhibitor for 11β-HSD1 and 11β-HSD2, were obtained from Sigma-Aldrich (St. Louis, MO). The recently developed 11β-HSD1 selective inhibitors 3-(1-adamantyl)-5,6,7,8,9,10-hexahydro[1,2,4]triazolo[4,3-α]azocine trifluoroacetate salt (WO03/065983, inhibitor A; Merck, Whitehouse Station, NJ; Ref. 23) and 2,4,6-trichloro-N-(5,5-dimethyl-7-oxo-4,5,6,7-tetrahydro-1,3-benzothiazol-2-yl) benzenesulfonamide (BVT-3498; Biovitrum, Stockholm, Sweden; Ref. 25) were synthesized according to the patent information.

Polyclonal antibodies against NF-κB p65, phospho-p65, p38 MAPK, phospho-p38, ERK1/2, phospho-ERK1/2, JNK, phospho-JNK, Akt, and phospho-Akt were purchased from Cell Signaling Technology (Beverly, MA). Polyclonal antibodies against SHIP1, PP2A, and MKP-1 were purchased from Santa Cruz Biotechnology (Santa Cruz, CA). An antibody against β-actin was purchased from Upstate Biotechnology (Lake Placid, NY). Horseradish peroxidase-conjugated anti-mouse, anti-rat, and anti-rabbit IgG antibodies and ECL Plus Western blotting detection kits were purchased from Amersham Biosciences (Piscataway, NJ).

Cell culture. 3T3-L1 cells (kindly provided by Dr. H. Green and Dr. M. Morikawa, Harvard Medical School, Boston, MA) were maintained in DMEM containing 10% (vol/vol) calf serum at 37°C under 10% CO_2.

Animals. Seventeen-week-old male C57BL/6 and nine-week-old *ob/ob* mice were used for the experiments. Mice were maintained on a standard diet (F-2, 3.7 kcal/g, 12% of kcal from fat, source soybean; Funahashi Farm) or a high-fat diet (Research Diets D12493, 5.2 kcal/g, 60% of kcal from fat, source soybean/lard) under a 14:10-h light-dark cycle at 23°C. The high-fat diet was administered to the diet-induced obese (DIO) mice from 3 to 17 wk of age. Animals were allowed free access to food and water. All animal experiments were undertaken in accordance with the guidelines for animal experiments of the Kyoto University Animal Research Committee.

Isolation of SVF and the mature adipocyte fraction. Subcutaneous (SQ), mesenteric (Mes), and epididymal (Epi) fat deposits were chopped using fine scissors and digested with 2 mg/ml collagenase (Type VIII; Sigma-Aldrich) in DMEM for 1 h at 37°C under continuous shaking (170 rpm). Dispersed tissue was filtered through a nylon mesh with a pore size of 250 μm and centrifuged. Digested material was separated by centrifugation at 1,800 rpm for 5 min. The sedimented SVF and cell supernatant [mature adipocyte fraction (MAF)] were both washed with DMEM. For primary culture experiments, SVF cells from epididymal fat pads were plated in sixwell plates and cultured overnight in DMEM containing 10% (vol/vol) FBS at 37°C under 10% CO_2. After being rinsed with the medium three times, the cells were incubated with or without TNF-α, carbenoxolone, or inhibitor A for 24 h.

Quantitative real-time PCR. Total RNA was extracted using Trizol reagent (Invitrogen, Carlsbad, CA), and cDNA was synthesized using an iScript cDNA synthesis kit (Bio-Rad, Hercules, CA) according to the manufacturer's instruction. The sequences of probes and primers are summarized in Suppl. Table S1 (supplemental data for this article are available at the *Am J Physiol Endocrinol Metab* website). Taqman PCR was performed using an ABI Prism 7300 sequence detection system following the manufacturer's instructions (Applied Biosystems, Foster City, CA). mRNA levels were normalized to those of 18S rRNA.

11β-HSD1 enzyme activity assay. 11β-HSD1 acts as a reductase and reactivates cortisol from cortisone in viable cells (54). In certain substrates, however, such as tissue homogenates or the microsome fraction, 11β-HSD1 acts as a dehydrogenase and inactivates cortisol to cortisone (8). 11β-HSD1 reductase activity in intact cells was measured as reported previously (8). Cells were incubated for 24 h in serum-free DMEM, with the addition of 250 nM cortisone and tritium-labeled tracer [1,2-^{3}H]$_2$-cortisone (Muromachi Yakuhin, Kyoto, Japan) for reductase activity and 250 nM cortisol with [1,2,6,7-^{3}H]$_4$-cortisol (Muromachi Yakuhin) for dehydrogenase activity. Cortisol and cortisone were extracted using ethyl acetate, evaporated, resuspended in ethanol, separated using thin-layer chromatography in 95:5 chloroform/methanol, and quantified using autoradiography.

To validate inhibitory potency of compounds against 11β-HSD1 with the use of FreeStyle 293 cells transiently transfected with human 11β-HSD1, the enzyme activity assay was carried out with 20 mM Tris · HCl at pH 7.0, 50 μM NADPH, 5 μg protein of microsomal fraction, and 300 nM [^{3}H]cortisone for 2 h. The reaction was stopped by 18β-glycyrrhetinic acid. The labeled cortisol product was captured by mouse monoclonal anti-cortisol antibody, bound to scintillation proximity assay beads coated with protein A, and quantified in a scintillation counter.

ELISA. Monocyte chemoattractant protein-1 (MCP-1) and IL-6 concentrations in the cultured media of 3T3-L1 preadipocytes were measured using ELISA according to the manufacturer's instructions (R&D Systems, Minneapolis, MN).

Western blot analysis. Two days after confluence, 3T3-L1 preadipocytes were stimulated with 10 ng/ml TNF-α in the absence or presence of 11β-HSD1 inhibitors (50 μM carbenoxolone or 10 μM inhibitor A) for 24 h.

For primary culture experiments, SVF from epididymal fat pads were plated in sixwell plates and cultured overnight in DMEM containing 10% (vol/vol) FBS at 37°C under 10% CO_2. After being rinsed with the medium three times, the cells were incubated with or without TNF-α, carbenoxolone, or inhibitor A for 24 h.

After 2-h serum starvation, cells were treated with TNF-α for 10 min to detect NF-κB and MAPK signals. Cells were washed with ice-cold PBS and harvested in lysis buffer (1% wt/vol SDS, 60 mM Tris · HCl, 1 mM Na$_3$VO$_4$, 0.1 mg/ml aprotinin, 1 mM PMSF, and 50 nM okadaic acid at pH 6.8) and boiled at 100°C for 10 min. After centrifugation, supernatants were normalized to the protein concentration via the Bradford method and then equal amounts of protein were subjected to SDS-PAGE and immunoblot analysis.

RNA interference. We tested four different small interfering RNA (siRNA) sequences. Stealth RNAi for mouse 11β-HSD1 (MSS205244, MSS205245, and MSS205246) (Invitrogen), and RNA interference (RNAi) for mouse 11β-HSD1 originally designed by an siRNA Design Support System (TaKaRa Bio, Shiga, Japan; sense: 5'-GAAAUGGCAUAUCAUCUGUTT-3' and antisense: 3'-TTCUUUACCGUAUAGUAGACA-5'). MSS205245 and MSS205246 did not suppress the 11β-HSD1 mRNA level effectively in preliminary experiments. Therefore, we demonstrated the data of MSS205244 [si(1)] and of the originally designed siRNA [si(2)] in this study. According to the manufacturer's protocol, 3T3-L1 preadipocytes were transfected with 10 nM siRNA in antibiotic-free medium using Lipofectamine RNAiMAX (Invitrogen). We assessed the ransfection efficiency using green fluorescent protein (GFP) detection (pmaxGFP), according to the manufacturer's instructions (Amaxa, Cologne, Germany). Fluorescent microscopic observa-

tion revealed that more than two-thirds of the cells expressed GFP (data not shown).

Expression vector. A mammalian expression vector encoding Hsd11b1 (Hsd11b1/pcDNA3.1) was constructed by inserting cDNA for mouse 11β-HSD1 into pcDNA3.1 (Invitrogen). 3T3-L1 preadipocytes were detached from culture dishes using 0.25% trypsin. Cells (5×10^6) were mixed with 2 μg plasmid in the solution provided with the cell line Nucleofector Kit V (Amaxa). pcDNA3.1/11β-HSD1 or a control vector was introduced into the cells using electroporation with a Nucleofector (Amaxa) instrument according to the manufacturer's instructions.

Statistical analysis. Data are expressed as the means ± SE of triplicate experiments. Data were analyzed using one-way ANOVA, followed by Student's *t*-tests for each pair of multiple comparisons. Differences were considered significant if $P < 0.05$.

RESULTS

Expression of 11β-HSD1 was elevated in the MAF and in SVF isolated from fat depots in ob/ob mice and DIO mice. Genetic (*ob/ob*) and dietary (DIO) obese models were analyzed. Expression of iNOS, MCP-1, and IL-6, all of which are obesity-related proinflammatory mediators (19, 29, 45, 56), was elevated in the MAF and SVF from both *ob/ob* mice and DIO mice compared with lean littermates (Fig. 1, *A* and *B*). Levels of 11β-HSD1 mRNA in the MAF from obese mice were substantially elevated compared with their lean littermates (*ob/ob*: SQ, 5-fold; Mes, 62-fold) (DIO: SQ, 24-fold; Mes, 460-fold; Fig. 1, *A* and *B*). On the other hand, levels of 11β-HSD1 mRNA in SVF from *ob/ob* mice and DIO mice were also elevated compared with their lean littermates (*ob/ob*: SQ, 3-fold; Mes, 3-fold; and DIO: SQ, 8-fold, Mes, 4-fold; Fig. 1, *A* and *B*).

TNF-α, IL-1β, and LPS augmented 11β-HSD1 mRNA expression and reductase activity in 3T3-L1 preadipocytes. When 3T3-L1 preadipocytes were treated with TNF-α (10

ng/ml) for 24 h, mRNA levels of 11β-HSD1 markedly increased (~4-fold; Fig. 2*iv*). Levels of iNOS, MCP-1, and IL-6 mRNA were concomitantly increased (50-, 70-, and 200-fold, respectively; Fig. 2, *i–iii*). IL-1β (1 ng/ml) and LPS (1,000 ng/ml) substantially augmented 11β-HSD1 mRNA expression in 3T3-L1 preadipocytes (10- and 3-fold vs. control, respectively) (Fig. 2*iv*). Reductase activity of 11β-HSD1 was augmented by TNF-α, IL-1β, and LPS compared with the control (2-, 9-, and 6-fold vs. control, respectively; $P < 0.05$; Fig. 2*v*). Based on the results of 11β-HSD1 activity, TNF-α was used at 10 ng/ml in subsequent experiments. On the other hand, 11β-HSD2 mRNA and the corresponding dehydrogenase activity were undetected not only at the baseline condition but with TNF-α, IL-1β, and LPS treatments (data not shown).

Dexamethasone decreased iNOS, MCP-1, and IL-6 mRNA and protein levels in TNF-α-treated 3T3-L1 preadipocytes. The effects of glucocorticoid on proinflammatory gene expression in TNF-α-treated 3T3-L1 preadipocytes were examined over a wide range of concentrations (10^{-10}, 10^{-9}, 10^{-8}, and 10^{-7} M), representing physiological to therapeutical levels in vivo (5). Dexamethasone (10^{-7} M) decreased mRNA levels of iNOS, MCP-1, and IL-6 (iNOS: 85 ± 2%, MCP-1: 40 ± 16%, and IL-6: 97 ± 1% reduction vs. TNF-α-treated cells) and protein levels in the media (MCP-1: 48 ± 5% and IL-6: 83 ± 1% reduction) in TNF-α-treated 3T3-L1 preadipocytes (Suppl. Fig. S1).

Pharmacological inhibition of 11β-HSD1 attenuated iNOS, MCP-1, and IL-6 mRNA and protein levels in TNF-α-treated 3T3-L1 preadipocytes. The effects of pharmacological inhibition of 11β-HSD1 on proinflammatory gene expression were examined in TNFα-treated 3T3-L1 preadipocytes. In previous in vitro studies, carbenoxolone (CBX), a nonselective inhibitor of 11β-HSD1 and 11β-HSD2, was used at concentrations from 5 to 300 μM (16, 17, 26). To date, an 11β-HSD1-specific
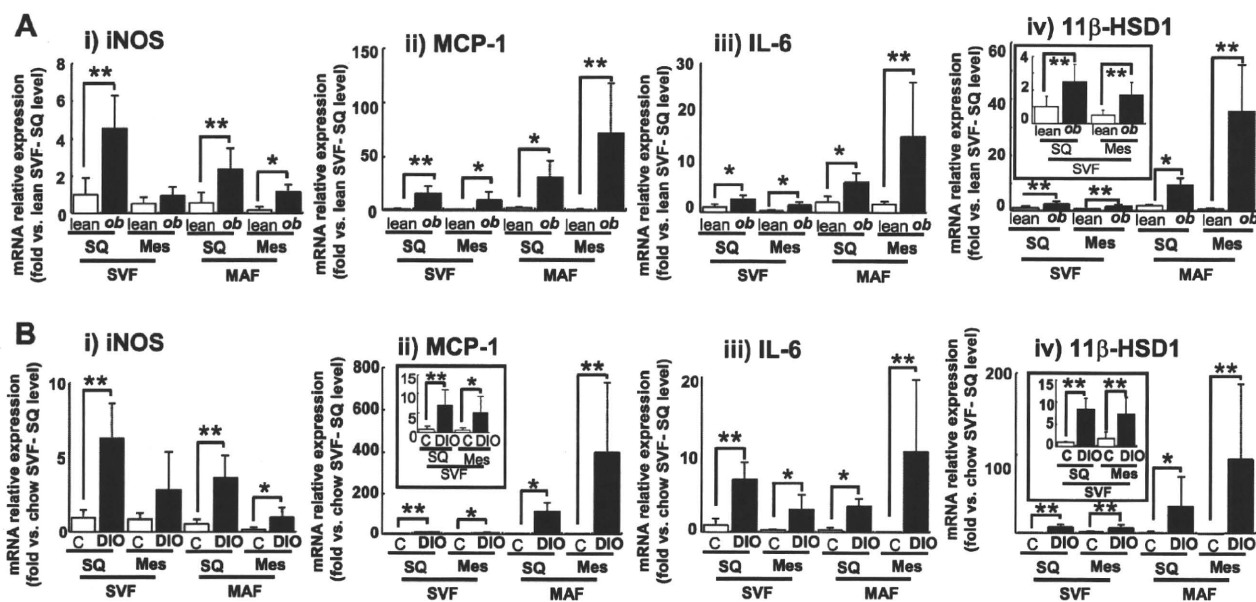

Fig. 1. 11β-Hydroxysteroid dehydrogenase type 1 (11β-HSD1) mRNA expression in stromal vascular fraction cells (SVF) and mature adipocytes fraction (MAF) isolated from obese adipose tissue of *ob/ob* mice and diet-induced obese (DIO) mice. *A*: *ob/ob* and lean littermates [control (C) 9 wk of age; *n* = 6]. *B*: DIO and littermates on a chow diet (17 wk of age; *n* = 6). Levels of inducible nitric oxide synthase (iNOS; *i*), monocyte chemoattractant protein-1 (MCP-1; *ii*), IL-6 (*iii*), and 11β-HSD1 (*iv*) mRNA in SVF and MAF in subcutaneous abdominal fat depots (SQ) and mesenteric fat depots (Mes). *$P < 0.05$, **$P < 0.01$ compared with lean littermates.
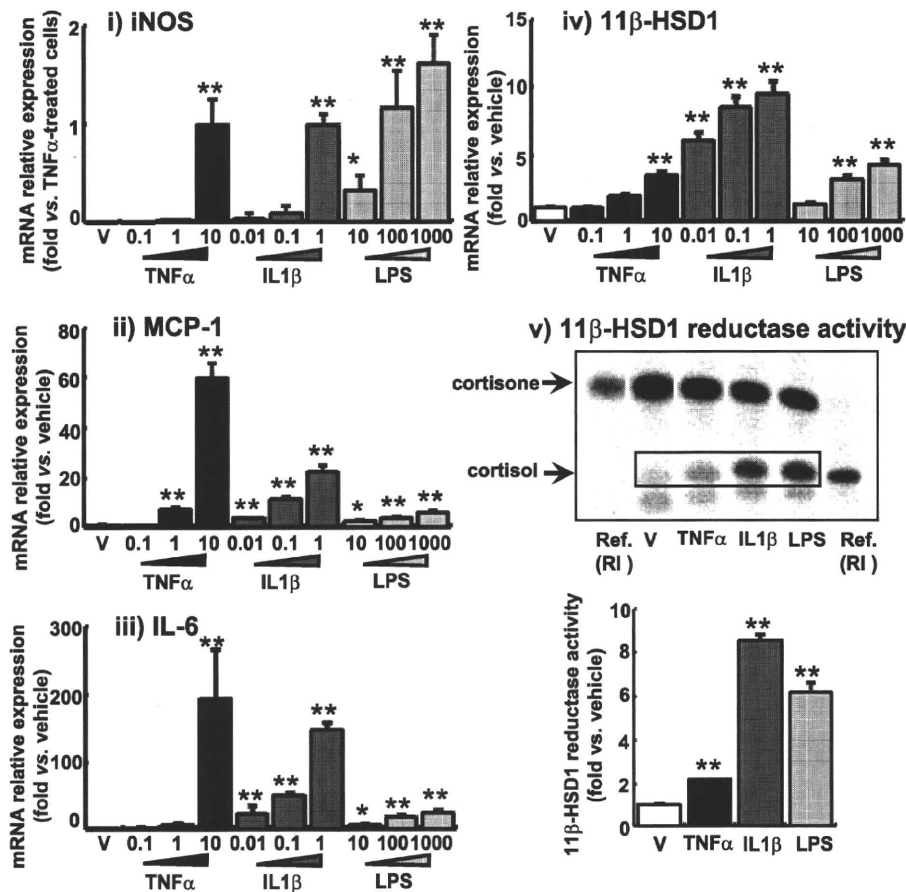
201

Fig. 2. TNF-α, IL-1β, and LPS augment the expression of proinflammatory mediators and 11β-HSD1 in 3T3-L1 preadipocytes. Cells were treated with TNF-α (0.1, 1, and 10 ng/ml), IL-1β, (0.01, 0.1, and 1 ng/ml) or LPS (10, 100, and 1,000 ng/ml) for 24 h. Levels of iNOS (*i*), MCP-1 (*ii*), IL-6 (*iii*), and 11β-HSD1 (*iv*) mRNA were quantified using real-time PCR. Values were normalized to that of 18S rRNA. *v*: 11β-HSD1 reductase activity (expressed as conversion ability of cortisone to cortisol) was assessed in the medium of 3T3-L1 cells treated with 10 ng/ml TNF-α, 1 ng/ml IL-1β, or 1,000 ng/ml LPS for 24 h. A reference of [³H]cortisone or [³H]cortisol was used as a size marker. A representative autoradiograph of thin-layer chromatography in 11β-HSD reductase activity assay (*top*) and quantification (*bottom*). Intensities of cortisol signals correspond to the enzyme activity of reductase. Ref. (RI), reference samples of [³H]cortisone or [³H]cortisol as size marker. Data are means ± SE of triplicate experiments. *$P < 0.05$, **$P < 0.01$, compared with vehicle (V)-treated group.

inhibitor, inhibitor A, has not been used for in vitro studies; however, another 11β-HSD1-specific inhibitor (compound 544) sharing almost the same structure as inhibitor A was used at a concentration of 5 μM (62). Therefore, in the present study, 10–50 μM CBX and 2.5–10 μM inhibitor A were used.

Before using these inhibitors in intact cells, we validated inhibitory potency of compounds against 11β-HSD1 in the microsome fraction assay. We verified that inhibitor A (10 nM) and CBX (1 μM) inhibited 11β-HSD1 activity as little as 25% vs. control, respectively, and that both of the 11β-HSD inhibitors suppressed 11β-HSD activity in a dose-dependent manner (Suppl. Fig. S2).

In 3T3-L1 preadipocytes, although CBX and inhibitor A did not change the level of 11β-HSD1 reductase activity, both of them suppressed TNF-α-induced reductase activity of 11β-HSD1 in a dose-dependent manner (Fig. 3A). CBX (50 μM) and inhibitor A (10 μM) markedly attenuated 11β-HSD1 activity (78 and 60% reduction vs. TNF-α-treated cells, respectively; Fig. 3A).

Without TNF-α-treatment, CBX and inhibitor A did not affect mRNA or protein levels of iNOS, MCP-1, and IL-6. On the other hand, in TNF-α-treated cells, these inhibitors reduced the mRNA and protein levels of proinflammatory genes. CBX decreased iNOS, MCP-1, and IL-6 mRNA levels (50 μM; iNOS: 83 ± 5%, MCP-1: 27 ± 4%, and IL-6: 47 ± 10% reduction vs. TNF-α-treated cells without compounds) and protein levels in the media (MCP-1: 17 ± 1% and IL-6: 34 ± 6% reduction) in TNF-α-treated 3T3-L1 preadipocytes (Fig.

3B). Similarly, inhibitor A reduced iNOS, MCP-1, and IL-6 mRNA (10 μM; iNOS: 47 ± 13%, MCP-1: 32 ± 12%, and IL-6: 33 ± 9% reduction) and protein levels in the media (MCP-1: 47 ± 3% and IL-6: 14 ± 3% reduction) (Fig. 3C).

Effect of 11β-HSD1 knockdown on proinflammatory properties in 3T3-L1 preadipocytes. To explore the potential role of 11β-HSD1 in cytokine release from activated preadipocytes, 11β-HSD1 was knocked down using siRNA. We tested four different siRNA sequences as described in MATERIALS AND METHODS; however, two of them did not suppress 11β-HSD1 mRNA level significantly in the preliminary experiments. Thus we demonstrated the data on si(1) and si(2).

When 3T3-L1 preadipocytes were transfected with 11β-HSD1 siRNA, TNF-α-induced expression of 11β-HSD1 was markedly attenuated [si(1): 60 ± 9% and si(2): 88 ± 7% reduction vs. negative control siRNA; Fig. 4A, *i*]. 11β-HSD1 reductase activity was also decreased by 11β-HSD1 siRNA [si(1): 81 ± 9% and si(2): 84 ± 3% reduction vs. negative control siRNA; Fig. 4A, *ii*]. 11β-HSD2 mRNA levels and the corresponding dehydrogenase activity were under detectable with or without siRNA treatments in 3T3-L1 preadipocytes (data not sown). Negative control RNAi did not influence the expression of 11β-HSD1. Knockdown of 11β-HSD1 in TNF-α-treated 3T3-L1 preadipocytes effectively reduced iNOS, MCP-1, and IL-6 mRNA levels [si(1): IL-6: 32 ± 7% reduction; and si(2): iNOS: 37 ± 8%, MCP-1: 22 ± 5%, and IL-6: 59 ± 3% reduction] and protein levels in the media [si(1):
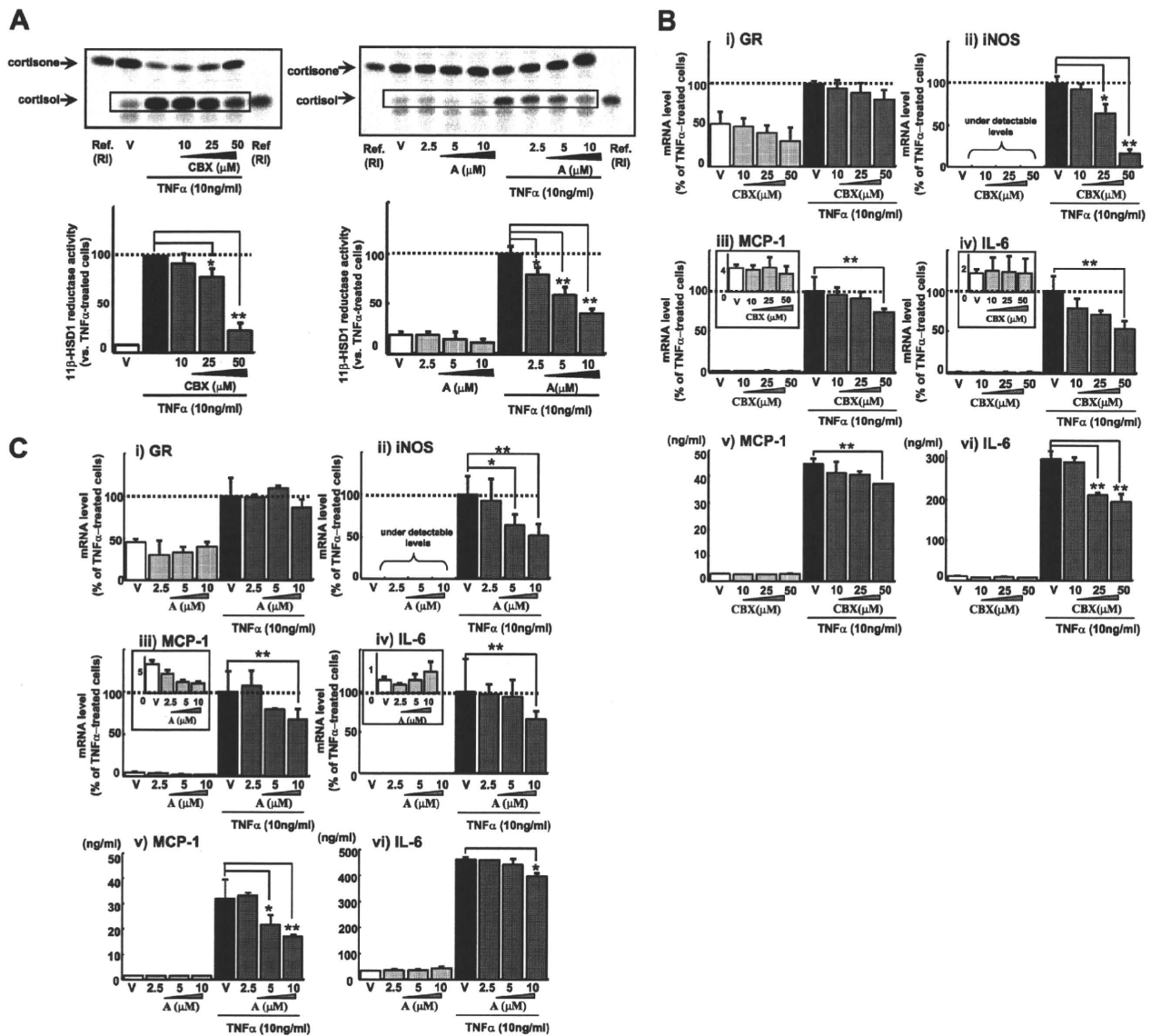
Fig. 3. Effects of pharmacological inhibition of 11β-HSD1 on glucocorticoid receptor (GR), MCP-1, IL-6, and iNOS expression in and secretion from TNF-α-treated 3T3-L1 preadipocytes. A: 11β-HSD1 activity assay for validation of 11β-HSD1 inhibitors. 3T3-L1 preadipocytes were incubated for 24 h in serum-free DMEM, adding 250 nM of cortisone with tritium-labeled cortisone. A representative autoradiograph of TLC for the 11β-HSD1 activity assay (top) and quantification of 11β-HSD1 activities (bottom). Intensities of cortisol signals correspond to the reductase activity. The y-axis shows percent 11β-HSD1 reductase activity compared with TNF-α (10 mg/ml)-treated cells. carbenoxolone (CBX; 10–50 μM) and inhibitor A (A; 2.5–10 μM) substantially reduced 11β-HSD1 activity in 3T3-L1 preadipocytes. CBX (B; 10–50 μM) and inhibitor A (C; 2.5–10 μM) 3T3-L1 preadipocytes were treated with TNF-α (10 ng/ml) or cotreated with CBX and inhibitor A for 24 h. GR (i), iNOS (ii), MCP-1 (iii), and IL-6 (iv) mRNA levels were determined using real-time PCR. Values were normalized to that of 18S rRNA and expressed relative to TNF-α-treated cells. Concentrations of MCP-1 (v) and IL-6 (vi) in the medium were measured with ELISA. Data are means ± SE of triplicate experiments. *$P < 0.05$, ** $P < 0.01$, compared with TNF-α-treated cells.

MCP-1: 13 ± 1% and IL-6: 17 ± 1% reduction; and si(2): MCP1: 19 ± 7% and IL-6: 30 ± 1% reduction; Fig. 4B].

Overexpression of 11β-HSD1 augmented iNOS, MCP-1, and IL-6 in TNF-α-treated 3T3-L1 preadipocytes. We examined whether overexpression of 11β-HSD1 is relevant to the augmentation of proinflammatory molecules in activated preadipocytes. The extent of 11β-HSD1 overexpression in 3T3-L1 preadipocytes was assessed by 11β-HSD1 mRNA levels and reductase activity (Fig. 5A). As expected, 11β-HSD1 mRNA level was increased by treatment of the 11β-HSD1 vector (~20-fold) or 10 ng/ml TNF-α (~300-fold) compared with the

vehicle. TNF-α-induced expression of 11β-HSD1 was further augmented by the introduction of the 11β-HSD1 vector (1.6-fold vs. empty vector). Reductase activity of 11β-HSD1 was also increased by the introduction of the vector (2-fold) or 10 ng/ml TNF-α (10-fold). Notably, TNF-α-induced enzyme activity was further augmented by the vector (1.3-fold vs. empty vector).

Expression of iNOS, MCP-1, and IL-6 did not differ between the 11β-HSD1 vector and the empty vector. On the other hand, TNF-α-induced expression of iNOS, MCP-1, and IL-6 was augmented in 11β-HSD1 transfectants (MCP-1: 172 ±
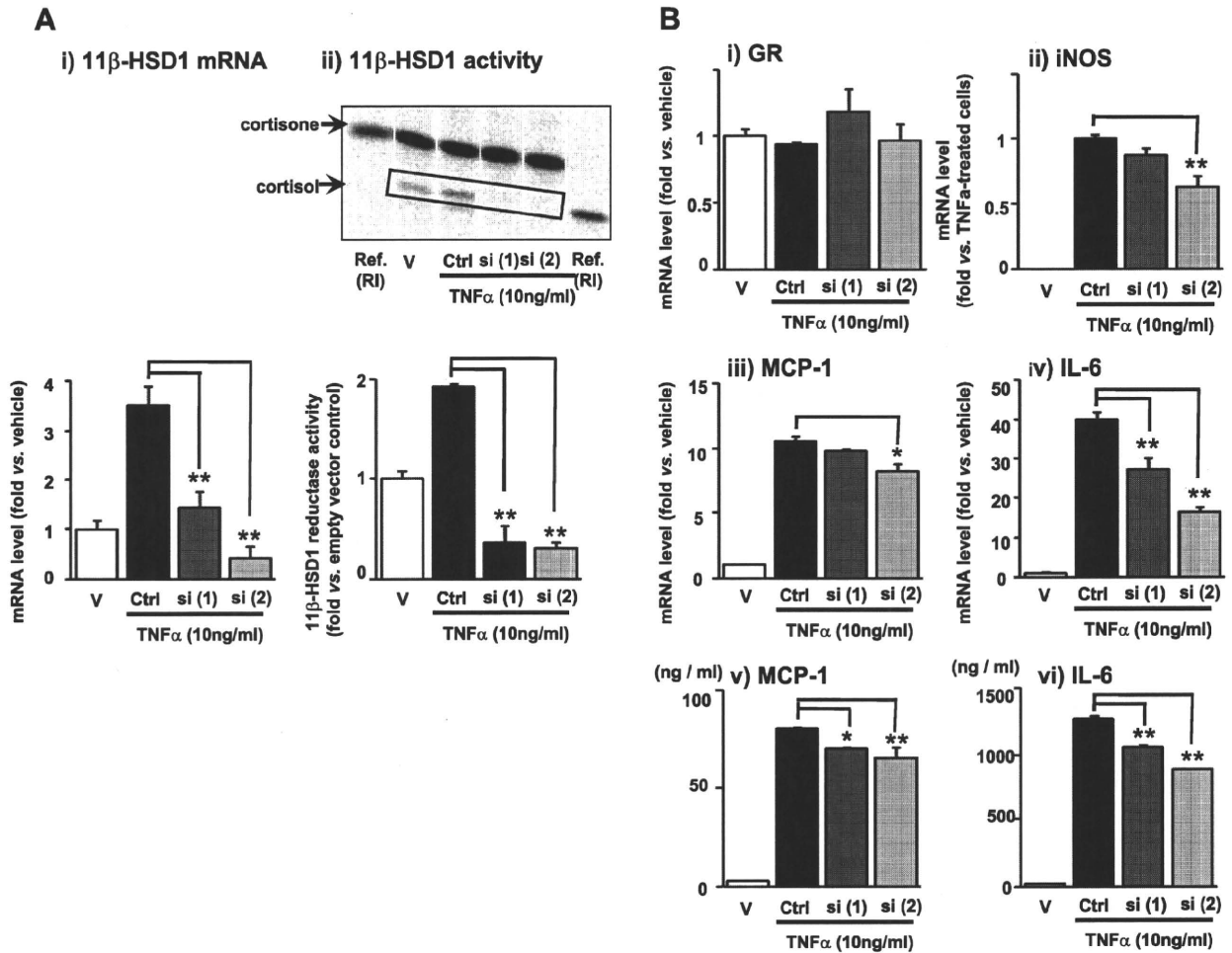
203

Fig. 4. Effects of 11β-HSD1 knockdown on TNF-α-induced expression of 11β-HSD1 in 3T3-L1 preadipocytes. Cells were transfected with either RNA interference for mouse 11β-HSD1 or a negative control (Ctrl). After 12 h incubation, cells were treated with 10 ng/ml TNF-α for 24 h. *A*: efficiency of 11β-HSD1 knockdown by small-interfering RNA. 11β-HSD1 mRNA (*i*) and reductase activity (*ii*). *B*: effects of knockdown of 11β-HSD1 on MCP-1, IL-6, and iNOS expression in and secretion from TNFα-treated 3T3-L1 preadipocytes. 11β-HSD1 (*i*), GR (*ii*), iNOS (*iii*), MCP-1 (*iv*), and IL-6 mRNA (*v*) levels were determined using real-time PCR. Values were normalized to that of 18S rRNA and expressed as a relative level vs. vehicle control (V). Concentrations of MCP-1 (*vi*) and IL-6 (*vii*) in the medium were measured with ELISA. Data are means ± SE of triplicate experiments. *P < 0.05, **P < 0.01, compared with TNF-α-treated cells. siRNA for mouse 11β-HSD1: si(1): MSS205244 (Invitrogen) and si(2): sense: 5′-GAAAUGGCAUAUCAUCUGUTT-3′ and antisense: 3′-TTCUUUACCGUAUAGUAGACA-5′ (Takara).

88%, IL-6: 194 ± 64%, and iNOS: 187 ± 47% vs. the empty vector; Fig. 5*B*, *ii-iv*). Similarly, protein levels of MCP-1 and IL-6 in the media were increased in transfectants (MCP-1: 206 ± 32% and IL-6: 156 ± 17% vs. the empty vector; Fig. 5*B*, *v* and *vi*).

Pharmacological inhibition of 11β-HSD1 attenuated TNF-α-induced NF-κB and MAPK signaling in 3T3-L1 preadipocytes. We examined the possible involvement of 11β-HSD1 in proinflammatory signaling pathways. 3T3-L1 preadipocytes were incubated with TNF-α (10 ng/ml), with or without CBX (50 μM) and inhibitor A (10 μM) for 24 h. After a 2-h serum starvation, the cells were incubated with TNF-α (10 ng/ml), with or without CBX (50 μM) and inhibitor A (10 μM) for 10 min. TNF-α-induced p-65 phosphorylation was markedly attenuated by CBX (30 ± 12% decrease vs. TNF-α-treated cells) and inhibitor A (51 ± 11% decrease vs. TNF-α-treated cells; Fig. 6*A*). Regarding MAPK signaling, augmented phosphorylation of p-38, JNK, and ERK with the TNF-α treatment was substantially attenuated by

CBX (p-38: 26 ± 8% decrease and JNK: 48 ± 3% decrease vs. TNF-α-treated cells) and inhibitor A (p-38: 51 ± 9% decrease, JNK: 72 ± 5% decrease, and ERK: 36 ± 11% decrease vs. TNF-α-treated cells; Fig. 6*B*).

Pharmacological inhibition of 11β-HSD1 attenuated iNOS, MCP-1, and IL-6 mRNA levels in SVF cells from ob/ob mice. We examined the effects of pharmacological inhibition of 11β-HSD1 on proinflammatory gene expression in primary cultured SVF cells isolated from epididymal fat depots in obese *ob/ob* mice or lean control mice.

CBX (50 μM) and inhibitor A (10 μM) did not change the expression level of 11β-HSD1 (Fig. 7*i*). CBX decreased mRNA level of iNOS, MCP-1, and IL-6 in both the basal state (iNOS: 69 ± 4%, MCP1: 42 ± 7%, and IL-6: 56 ± 14% reduction vs. vehicle control) and TNFα-stimulated state (iNOS: 58 ± 11%, MCP-1: 63 ± 5%, and IL-6: 53 ± 8% reduction vs. TNFα-treated cells without compounds) in SVF cells from *ob/ob* mice.

204

A

i) 11β-HSD1 mRNA　　ii) 11β-HSD1 activity

B

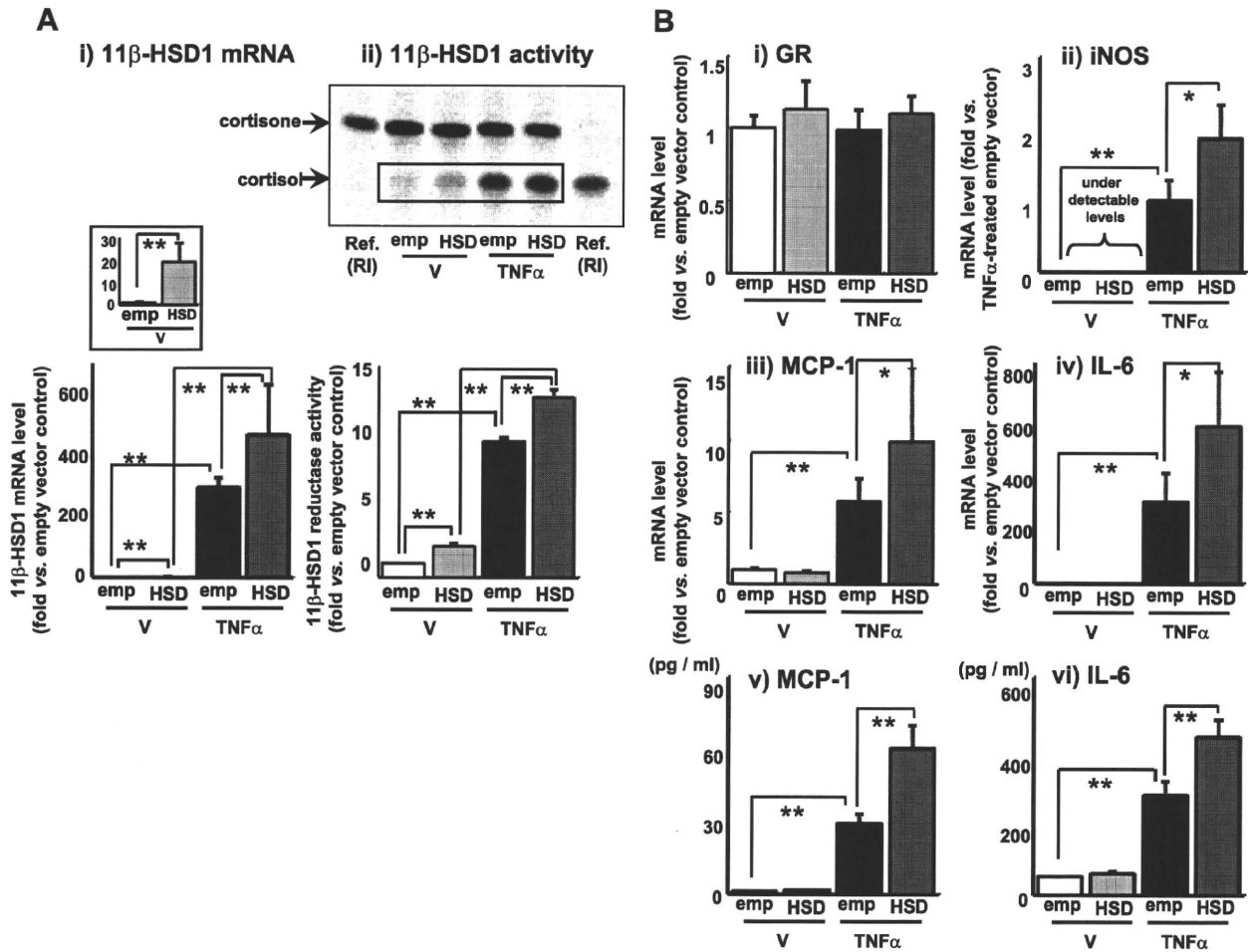### i) GR　　　ii) iNOS

iii) MCP-1　　iv) IL-6

v) MCP-1　　vi) IL-6

Fig. 5. Effects of overexpression of 11β-HSD1 on MCP-1, IL-6, and iNOS expression in and secretion from TNF-α-treated 3T3-L1 preadipocytes. *A*: efficiency of electroporation-mediated gene transfer. 3T3-L1 preadipocytes were transfected with the expression vector for 11β-HSD1 or a corresponding empty vector using electroporation. After 48 h, cells were treated with or without 10 ng/ml TNF-α for 24 h. Cells were assayed for 11β-HSD1 mRNA (*i*) and reductase activity (*ii*). *B*: effects of overexpression of 11β-HSD1 on MCP-1, IL-6, and iNOS expression in and secretion from TNF-α-treated 3T3-L1 preadipocytes. 3T3-L1 preadipocytes were transfected as above, and 48 h after the infection, cells were treated with or without 10 ng/ml TNF-α for 24 h. Levels of mRNA for GR (*i*), iNOS (*ii*), MCP-1 (*iii*), and IL-6 (*iv*) were determined using real-time PCR. Values were normalized to those of 18S rRNA and expressed as a relative level vs. the vehicle control (V). Concentrations of MCP-1 (*v*) and IL-6 (*vi*) in the medium were measured with ELISA. Data are means ± SE of triplicate experiments. *$P < 0.05$, **$P < 0.01$.

Without TNF-α-treatment, CBX did not change mRNA levels of iNOS, MCP-1 and IL-6 in SVF cells from lean control mice. However, CBX reduced the mRNA levels of iNOS, MCP-1, and IL-6 (iNOS: 64 ± 18%, MCP-1: 67 ± 14%, and IL-6: 58 ± 12% reduction vs. TNF-α-treated cells without compounds) in TNF-α-treated SVF cells from lean control mice (Fig. 7).

Pharmacological inhibition of 11β-HSD1 attenuated NF-κB and MAPK signaling in SVF cells from ob/ob mice. SVF cells from *ob/ob* or lean control mice were incubated with TNF-α (10 ng/ml), with or without CBX (50 μM) and inhibitor A (10 μM) for 24 h. After a 2-h serum starvation, the cells were incubated with TNF-α (10 ng/ml), with or without CBX (50 μM) and inhibitor A (10 μM) for 10 min. Activation of NF-κB (p65) and MAPK (p38, JNK, and ERK) signaling did occur in SVF cells from *ob/ob* mice compared with lean control (Suppl. Fig. S3). In *ob/ob* mice, phosphorylation of these signaling without TNF-α treatment was attenuated by CBX and inhibitor A. TNF-α-induced p-65,

p38, JNK, and ERK phosphorylation was also attenuated by CBX and inhibitor A in SVF cells from both *ob/ob* and lean control mice (Suppl. Fig. S3).

DISCUSSION

Here we provide novel evidence that inflammatory stimuli-induced 11β-HSD1 in activated preadipocytes intensifies NF-κB and MAPK signaling pathways and the resultant augmentation of proinflammatory molecules. Not limited to 3T3-L1 preadipocytes, we also demonstrated the notion was reproducible in the primary SVF cells from obese mice. Previous works focused on the metabolically beneficial impact of 11β-HSD1 deficiency on adipose tissue distribution, fuel homeostasis, and insulin sensitivity. On the other hand, clearly distinct from previous works, our present study is the first to highlight an unexpected, proinflammatory role of reamplified glucocorticoids within activated preadipocytes in obese adipose tissue.
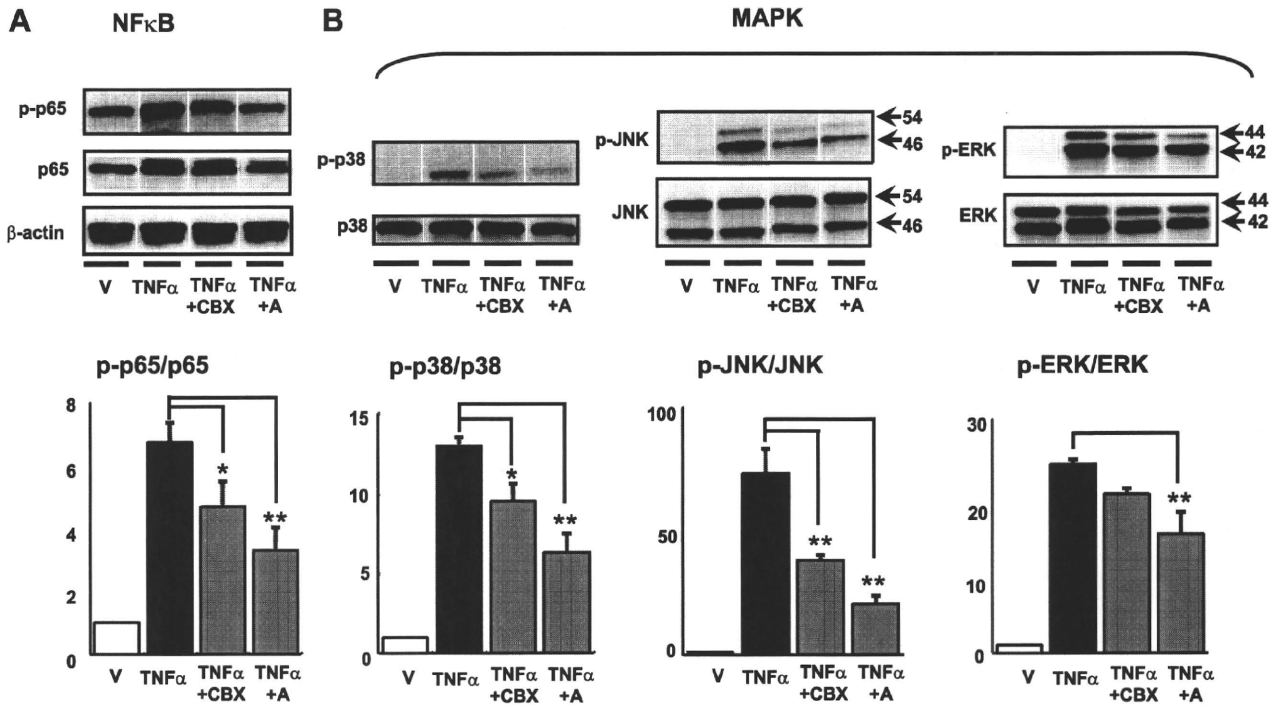
205

Fig. 6. Effects of inhibition of 11β-HSD1 on TNF-α-induced NFκB and MAPK signaling. NFκB (*A*) and MAPK (*B*) signaling pathways. 3T3-L1 preadipocytes were treated with 10 ng/ml TNF-α for 24 h in the presence or absence of 11β-HSD1 inhibitors (CBX or inhibitor A). After 2-h serum starvation, cells were treated with TNF-α in the presence or absence of 11β-HSD1 inhibitors for 10 min to assess the activation of NFκB and MAPK signaling pathways. Western blot analyses were performed using antibodies against β-actin and NFκB-p65 (*A*), phospho-p65 (*B*), p38-MAPK (*B, left*), phospho-p38 (*B, center*) JNK, phospho-JNK (*B, right*) ERK 1/2, and phospho-ERK1/2. A representative Western blot (*top*) and quantification of p65, p38, JNK, and ERK phosphorylation (*bottom*). Data are means ± SE of triplicate experiments. *$P < 0.05$, **$P < 0.01$ compared with TNF-α-treated cells.

Suppression and overexpression experiments with 11β-HSD1 in activated preadipocytes demonstrate that TNF-α-induced 11β-HSD1 further augments the expression of proinflammatory genes including iNOS, MCP-1, and IL-6. Elevation of iNOS, MCP-1, and IL-6 in adipose tissue is commonly observed in obese subjects, linking to dysfunction of adipose tissue (19, 29, 45, 56). For example, iNOS-deficient mice are protected against obesity-induced insulin resistance and glucose intolerance (45). Moreover, transgenic mice overexpressing MCP-1 in adipose tissue exemplify insulin resistance and exaggerated infiltration of macrophages into adipose tissue (29). Previous studies (20, 36) showed that adipose tissue is a primary production site for IL-6 in humans. In fact, circulating IL-6 levels are shown to elevate in patients with insulin-resistance (19, 56), impaired glucose tolerance (40), and type 2 diabetes (47). Taken together, the present study provides novel evidence for proinflammatory role of 11β-HSD1 in activated preadipocytes.

To optimize experimental condition, the present study was designed to eliminate possible toxic effects and nonspecific effects of 11β-HSD1 inhibitors. Because 11β-HSD2 mRNA and corresponding dehydrogenase enzyme activity (8, 27) were undetected in 3T3-L1 preadipocytes even after the treatment with TNF-α (unpublished observations), CBX virtually serves as a specific inhibitor against 11β-HSD1 in the present study. To further verify the effect of 11β-HSD1 inhibition on activated preadipocytes, we confirmed that an 11β-HSD1-specific inhibitor A exerted similar effects to CBX (Fig. 3). Of note, the expression level of the glucocorticoid receptor did not vary by

the treatment with 11β-HSD1 inhibitors (unpublished observations). The notion that TNF-α-induced 11β-HSD1 would reinforce the expression of proinflammatory genes was endorsed by the results of RNAi experiments (Fig. 4) and overexpression experiments (Fig. 5). It should be emphasized that forced overexpression of 11β-HSD1 per se did not influence the expression level of proinflammatory genes in nonactivated preadipocytes (Fig. 5B). These findings led us to speculate that 11β-HSD1-mediated active glucoorticoids within cells reinforce inflammation under proinflammatory conditions commonly seen in obese adipose tissue.

The present study demonstrated that 11β-HSD1 was highly expressed in SVF cells from obese adipose tissue (Fig. 1). Although mature adipocytes abundantly express 11β-HSD1 (44, 61), a considerable amount of 11β-HSD1 expression was detected in SVF from adipose tissue (Fig. 1). Potential link between preadipocyte function and pathophysiology of obese adipose tissue has recently attracted research interest (53, 57). A recent study (14) using 11β-HSD1 knockout mice provided evidence that 11β-HSD1 in preadipocytes may affect fat distribution under overnutrition. In 3T3-L1 cells, the expression level of 11β-HSD1 is lower in preadipocytes but is dramatically increased during the course of differentiation into mature adipocytes (51). In fact, active glucocorticoids generated intracellularly by 11β-HSD1 are critical for normal adipose differentiation (33). On the other hand, TNF-α augments 11β-HSD1 expression in preadipocytes (Fig. 2). Of note, in proinflammatory milieu, TNF-α inhibits adipocyte differentiation by decreasing PPARγ expression (43, 46, 64). Depending on the
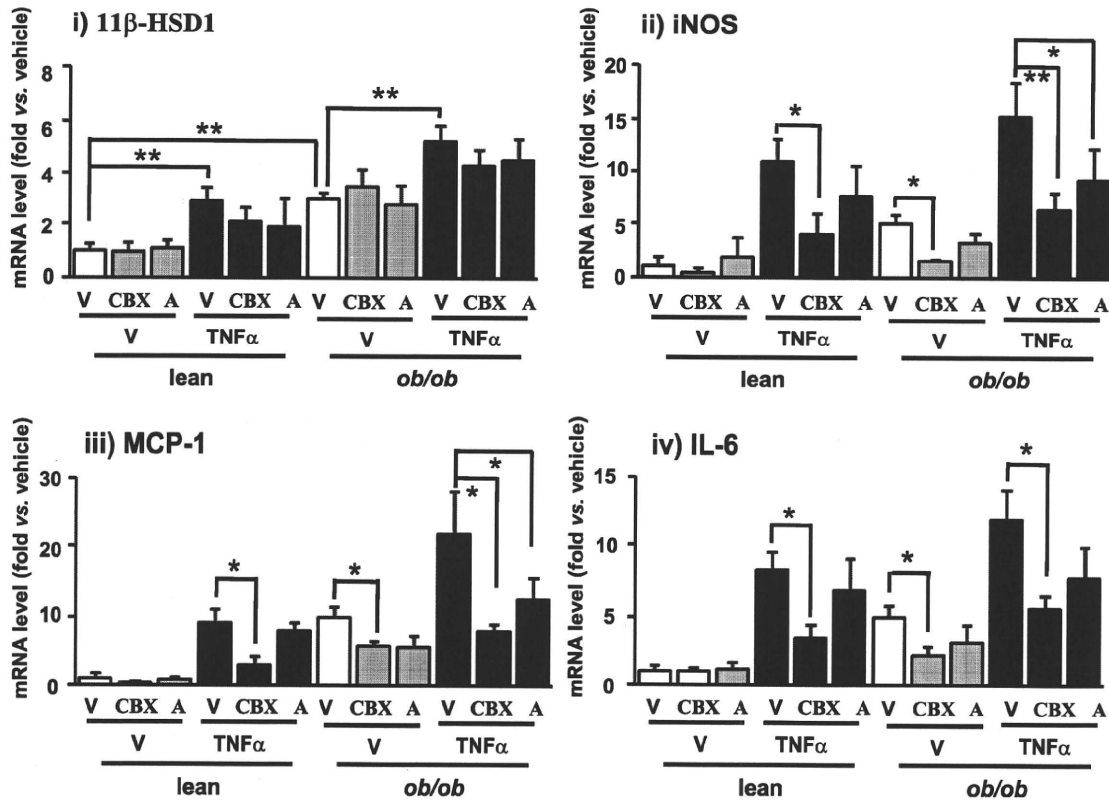
Fig. 7. Effects of pharmacological inhibition of 11β-HSD1 on iNOS, MCP-1, and IL-6 mRNA levels in SVF cells from *ob/ob* mice. SVF cells from *ob/ob* mice and lean control mice were treated with CBX (50 μM) or inhibitor A (10 μM), with or without TNF-α (10 ng/ml) for 24 h. 11β-HSD1 (*i*), iNOS (*ii*), MCP-1 (*iii*), and IL-6 mRNA (*iv*) levels were determined using real-time PCR. Values were normalized to that of 18S rRNA and expressed relative to lean control. Data are means ± SE of triplicate experiments. *$P < 0.05$, **$P < 0.01$.

hormonal milieu, it is therefore conceivable that 11β-HSD1 plays a role in both adipogenesis and inflammatory response in preadipoytes.

We assessed the expression of Pref-1 (a representative molecular marker for preadipocytes; Ref. 7) as well as aP2, PPARγ2, and GLUT4 (a set of representative markers for differentiated adipocytes; Refs. 32 and 59) in preadipocytes overexpressing 11β-HSD1. Consequently, forced augmentation of 11β-HSD1 did not affect the expression level of these genes (Suppl. Fig. S4), supporting that a line of our observation was not a facet of mature adipocytes but of preadipocytes.

Previous studies demonstrated that chronic inflammation is closely associated with insulin resistance in insulin-sensitive organs (24, 64). Glucocorticoids are widely used as anti-inflammatory agents in a clinical setting (49). On the other hand, this hormone simultaneously causes insulin resistance (4, 50). Regarding this apparent paradox, recent studies (34, 55) suggest that reactivated glucocorticoids within cells have the potential to enhance inflammatory or immune responses in a variety of cells. In the present study, replenished dexamethasone in the culture media at pharmacological doses did decrease the synthesis and secretion of proinflammatory molecules in preadipocytes in a dose-dependent manner (Fig. 3). On the other hand, in activated preadipocytes, 11β-HSD1 intensifies TNF-α-induced activation of NF-κB and the MAPK signaling cascade (Fig. 6). In this context, it is possible that intracellular activation of glucocorticoids within physiological range would likely cause proinflammatory responses in certain

cell types. It should be noted that preadipocytes possess very few insulin receptors (51). Instead, preadipocytes express a large number of IGF-1 receptors (18). Insulin can bind to the IGF-1 receptor only at supraphysiological concentrations. However, it is likely that increased release of inflammatory cytokines from activated preadipocytes may aggravate insulin receptor signaling in adjacent mature adipocytes in obese adipose tissue. This notion is supported by a line of mouse experiments showing that pharmacological inhibition of 11β-HSD1 ameliorated diabetes, dyslipidemia, and even arteriosclerosis (1, 23).

PPARγ agonists potently suppress the activity of 11β-HSD1 exclusively in adipose tissue (6). The present finding that amplified glucocorticoids within activated preadipocytes may enhance inflammatory responses does not contradict the notion that PPARγ agonists exert potent anti-inflammatory effects in a variety of cell types (37).

Recent studies showed that phosphoinositide 3-kinase (PI3K)-Akt pathways, IL-1 receptor-associated kinase-M (IRAK-M), and suppressors of cytokine signaling-1 (SOCS-1) are negative regulators of NF-κB and MAPK signaling (21). Under inflammatory stimuli, a physiological dose of glucocorticoids positively regulates the expression of SHIP1, a phosphatase that negatively regulates PI3K signaling, resulting in the activation of NF-κB and MAPK in activated macrophages (67). Considering the close biological similarities between activated preadipocytes and activated macrophages (11, 13), we explored whether PI3K-Akt pathways, SHIP1, or other phosphatases could be

involved in the 11β-HSD1-induced NF-κB and MAPK activation. Western blot analyses indicated that phosphorylation of Akt or protein levels of SHIP1, PP2A, or MKP-1 did not change significantly with inhibition or overexpression of 11β-HSD1 (Suppl. Fig. S5). Further studies are warranted to unravel the entire mechanism.

In summary, the present study provides novel evidence that inflammatory stimuli-induced 11β-HSD1 reinforces NF-κB and MAPK signaling pathways and results in further induction of proinflammatory molecules in activated preadipocytes. Our findings highlight an unexpected, inflammatory role of reactivated glucocorticoids within preadipocytes in obese adipose tissue.

REFERENCES

1. **Alberts P, Nilsson C, Selen G, Engblom LO, Edling NH, Norling S, Klingstrom G, Larsson C, Forsgren M, Ashkzari M, Nilsson CE, Fiedler M, Bergqvist E, Ohman B, Bjorkstrand E, Abrahmsen LB.** Selective inhibition of 11 beta-hydroxysteroid dehydrogenase type 1 improves hepatic insulin sensitivity in hyperglycemic mice strains. *Endocrinology* 144: 4755–4762, 2003.
2. **Andrew R, Phillips DI, Walker BR.** Obesity and gender influence cortisol secretion and metabolism in man. *J Clin Endocrinol Metab* 83: 1806–1809, 1998.
3. **Andrews RC, Rooyackers O, Walker BR.** Effects of the 11 beta-hydroxysteroid dehydrogenase inhibitor carbenoxolone on insulin sensitivity in men with type 2 diabetes. *J Clin Endocrinol Metab* 88: 285–291, 2003.
4. **Asensio C, Muzzin P, Rohner-Jeanrenaud F.** Role of glucocorticoids in the physiopathology of excessive fat deposition and insulin resistance. *Int J Obes Relat Metab Disord* 28 Suppl 4: S45–52, 2004.
5. **Balachandran A, Guan H, Sellan M, van Uum S, Yang K.** Insulin and dexamethasone dynamically regulate adipocyte 11beta-hydroxysteroid dehydrogenase type 1. *Endocrinology* 149: 4069–4079, 2008.
6. **Berger J, Tanen M, Elbrecht A, Hermanowski-Vosatka A, Moller DE, Wright SD, Thieringer R.** Peroxisome proliferator-activated receptor-gamma ligands inhibit adipocyte 11beta-hydroxysteroid dehydrogenase type 1 expression and activity. *J Biol Chem* 276: 12629–12635, 2001.
7. **Boney CM, Fiedorek FT Jr, Paul SR, Gruppuso PA.** Regulation of preadipocyte factor-1 gene expression during 3T3–L1 cell differentiation. *Endocrinology* 137: 2923–2928, 1996
8. **Bujalska IJ, Kumar S, Stewart PM.** Does central obesity reflect "Cushing's disease of the omentum"? *Lancet* 349: 1210–1213, 1997.
9. **Cancello R, Henegar C, Viguerie N, Taleb S, Poitou C, Rouault C, Coupaye M, Pelloux V, Hugol D, Bouillot JL, Bouloumie A, Barbatelli G, Cinti S, Svensson PA, Barsh GS, Zucker JD, Basdevant A, Langin D, Clement K.** Reduction of macrophage infiltration and chemoattractant gene expression changes in white adipose tissue of morbidly obese subjects after surgery-induced weight loss. *Diabetes* 54: 2277–2286, 2005.
10. **Chapman KE, Coutinho AE, Gray M, Gilmour JS, Savill JS, Seckl JR.** The role and regulation of 11beta-hydroxysteroid dehydrogenase type 1 in the inflammatory response. *Mol Cell Endocrinol* 301: 123–131, 2009.
11. **Charriere G, Cousin B, Arnaud E, Andre M, Bacou F, Penicaud L, Casteilla L.** Preadipocyte conversion to macrophage. Evidence of plasticity. *J Biol Chem* 278: 9850–9855, 2003.
12. **Chung S, Lapoint K, Martinez K, Kennedy A, Boysen Sandberg M, McIntosh MK.** Preadipocytes mediate lipopolysaccharide-induced in-

flammation and insulin resistance in primary cultures of newly differentiated human adipocytes. *Endocrinology* 147: 5340–5351, 2006.
13. **Cousin B, Munoz O, Andre M, Fontanilles AM, Dani C, Cousin JL, Laharrague P, Casteilla L, Penicaud L.** A role for preadipocytes as macrophage-like cells. *FASEB J* 13: 305–312, 1999.
14. **De Sousa Peixoto RA, Turban S, Battle JH, Chapman KE, Seckl JR, Morton NM.** Preadipocyte 11beta-hydroxysteroid dehydrogenase type 1 is a keto-reductase and contributes to diet-induced visceral obesity in vivo. *Endocrinology* 149: 1861–1868, 2008.
16. **Dembinska-Kiec A, Pallapies D, Simmet T, Peskar BM, Peskar BA.** Effect of carbenoxolone on the biological activity of nitric oxide: relation to gastroprotection. *Br J Pharmacol* 104: 811–816, 1991.
17. **Elsen FP, Shields EJ, Roe MT, Vandam RJ, Kelty JD.** Carbenoxolone induced depression of rhythmogenesis in the pre-Botzinger complex. *BMC Neurosci* 9: 46, 2008.
18. **Entingh-Pearsall A, Kahn, CR.** Differential roles of the insulin and insulin-like growth factor-i (igf-i) receptors in response to insulin and IGF-I. *J Biol Chem* 279: 38016–38024, 2004.
19. **Fernandez-Real JM, Vayreda M, Richart C, Gutierrez C, Broch M, Vendrell J, Ricart W.** Circulating interleukin 6 levels, blood pressure, and insulin sensitivity in apparently healthy men and women. *J Clin Endocrinol Metab* 86: 1154–1159, 2001.
20. **Fried SK, Bunkin DA, Greenberg AS.** Omental and subcutaneous adipose tissues of obese subjects release interleukin-6: depot difference and regulation by glucocorticoid. *J Clin Endocrinol Metab* 83: 847–850, 1998.
21. **Fukao T, Koyasu S.** PI3K and negative regulation of TLR signaling. *Trends Immunol* 24: 358–363, 2003.
22. **Hauner H.** Secretory factors from human adipose tissue and their functional role. *Proc Nutr Soc* 64: 163–169, 2005.
23. **Hermanowski-Vosatka A, Balkovec JM, Cheng K, Chen HY, Hernandez M, Koo GC, Le Grand CB, Li Z, Metzger JM, Mundt SS, Noonan H, Nunes CN, Olson SH, Pikounis B, Ren N, Robertson N, Schaeffer JM, Shah K, Springer MS, Strack AM, Strowski M, Wu K, Wu T, Xiao J, Zhang BB, Wright SD, Thieringer R.** 11beta-HSD1 inhibition ameliorates metabolic syndrome and prevents progression of atherosclerosis in mice. *J Exp Med* 202: 517–527, 2005.
24. **Hotamisligil GS.** Inflammation and metabolic disorders. *Nature* 444: 860–867, 2006.
25. **Hult M, Shafqat N, Elleby B, Mitschke D, Svensson S, Forsgren M, Barf T, Vallgarda J, Abrahmsen L, Oppermann U.** Active site variability of type 1 11beta-hydroxysteroid dehydrogenase revealed by selective inhibitors and cross-species comparisons. *Mol Cell Endocrinol* 248: 26–33, 2006.
26. **Ishii T, Masuzaki H, Tanaka T, Arai N, Yasue S, Kobayashi N, Tomita T, Noguchi M, Fujikura J, Ebihara K, Hosoda K, Nakao K.** Augmentation of 11beta-hydroxysteroid dehydrogenase type 1 in LPS-activated J774.1 macrophages–role of 11beta-HSD1 in pro-inflammatory properties in macrophages. *FEBS Lett* 581: 349–354, 2007.
27. **Jamieson PM, Chapman KE, Edwards CR, Seckl JR.** 11 beta-hydroxysteroid dehydrogenase is an exclusive 11 beta- reductase in primary cultures of rat hepatocytes: effect of physicochemical and hormonal manipulations. *Endocrinology* 136: 4754–4761, 1995.
28. **Julien P, Despres JP, Angel A.** Scanning electron microscopy of very small fat cells and mature fat cells in human obesity. *J Lipid Res* 30: 293–299, 1989.
29. **Kanda H, Tateya S, Tamori Y, Kotani K, Hiasa K, Kitazawa R, Kitazawa S, Miyachi H, Maeda S, Egashira K, Kasuga M.** MCP-1 contributes to macrophage infiltration into adipose tissue, insulin resistance, and hepatic steatosis in obesity. *J Clin Invest* 116: 1494–1505, 2006.
30. **Kershaw EE, Morton NM, Dhillon H, Ramage L, Seckl JR, Flier JS.** Adipocyte-specific glucocorticoid inactivation protects against diet-induced obesity. *Diabetes* 54: 1023–1031, 2005.
31. **Kotelevtsev Y, Holmes MC, Burchell A, Houston PM, Schmoll D, Jamieson P, Best R, Brown R, Edwards CR, Seckl JR, Mullins JJ.** 11beta-hydroxysteroid dehydrogenase type 1 knockout mice show attenuated glucocorticoid-inducible responses and resist hyperglycemia on obesity or stress. *Proc Natl Acad Sci USA* 94: 14924–14929, 1997.
32. **Lane MD, Tang QQ, Jiang MS.** Role of the CCAAT enhancer binding proteins (C/EBPs) in adipocyte differentiation. *Biochem Biophys Res Commun* 266: 677–683, 1999.

208

33. **Liu Y, Sun Y, Zhu T, Xie Y, Yu J, Sun WL, Ding GX, Hu G.** 11β HSD1 promotes differentiation of 3T3-L1 preadipocyte. *Acta Pharmacol Sin* 28: 1198–204, 2007.

34. **McEwen BS, Biron CA, Brunson KW, Bulloch K, Chambers WH, Dhabhar FS, Goldfarb RH, Kitson RP, Miller AH, Spencer RL, Weiss JM.** The role of adrenocorticoids as modulators of immune function in health and disease: neural, endocrine and immune interactions. *Brain Res Brain Res Rev* 23: 79–133, 1997.

35. **McLaughlin T, Sherman A, Tsao P, Gonzalez O, Yee G, Lamendola C, Reaven GM, Cushman SW.** Enhanced proportion of small adipose cells in insulin-resistant vs insulin-sensitive obese individuals implicates impaired adipogenesis. *Diabetologia* 50: 1707–1715, 2007.

36. **Mohamed-Ali V, Goodrick S, Rawesh A, Katz DR, Miles JM, Yudkin JS, Klein S, Coppack SW.** Subcutaneous adipose tissue releases interleukin-6, but not tumor necrosis factor-alpha, in vivo. *J Clin Endocrinol Metab* 82: 4196–4200, 1997.

37. **Moller DE, Berger JP.** Role of PPARs in the regulation of obesity-related insulin sensitivity and inflammation. *Int J Obes Relat Metab Disord* 27 Suppl 3: S17–21, 2003.

38. **Montague CT, O'Rahilly S.** The perils of portliness: causes and consequences of visceral adiposity. *Diabetes* 49: 883–888, 2000.

39. **Morton NM, Paterson JM, Masuzaki H, Holmes MC, Staels B, Fievet C, Walker BR, Flier JS, Mullins JJ, Seckl JR.** Novel adipose tissue-mediated resistance to diet-induced visceral obesity in 11β-hydroxysteroid dehydrogenase type 1-deficient mice. *Diabetes* 53: 931–938, 2004.

40. **Muller S, Martin S, Koenig W, Hanifi-Moghaddam P, Rathmann W, Haastert B, Giani G, Illig T, Thorand B, Kolb H.** Impaired glucose tolerance is associated with increased serum concentrations of interleukin 6 and co-regulated acute-phase proteins but not TNF-alpha or its receptors. *Diabetologia* 45: 805–812, 2002.

41. **Napolitano A, Voice MW, Edwards CR, Seckl JR, Chapman KE.** 11beta-hydroxysteroid dehydrogenase 1 in adipocytes: expression is differentiation-dependent and hormonally regulated. *J Steroid Biochem Mol Biol* 64: 251–260, 1998.

42. **Ohara Y, Peterson TE, Harrison DG.** Hypercholesterolemia increases endothelial superoxide anion production. *J Clin Invest* 91: 2546–2551, 1993.

43. **Pape ME, Kim KH.** Effect of tumor necrosis factor on acetyl-coenzyme A carboxylase gene expression and preadipocyte differentiation. *Mol Endocrinol* 2: 395–403, 1988.

44. **Paulmyer-Lacroix O, Boullu S, Oliver C, Alessi MC, Grino M.** Expression of the mRNA coding for 11beta-hydroxysteroid dehydrogenase type 1 in adipose tissue from obese patients: an in situ hybridization study. *J Clin Endocrinol Metab* 87: 2701–2705, 2002.

45. **Perreault M, Marette A.** Targeted disruption of inducible nitric oxide synthase protects against obesity-linked insulin resistance in muscle. *Nat Med* 7: 1138–1143, 2001.

46. **Petruschke T, Hauner H.** Tumor necrosis factor-alpha prevents the differentiation of human adipocyte precursor cells and causes delipidation of newly developed fat cells. *J Clin Endocrinol Metab* 76: 742–747, 1993.

47. **Pickup JC, Mattock MB, Chusney GD, Burt D.** NIDDM as a disease of the innate immune system: association of acute-phase reactants and interleukin-6 with metabolic syndrome X. *Diabetologia* 40: 1286–1292, 1997.

48. **Poulain-Godefroy O, Froguel P.** Preadipocyte response and impairment of differentiation in an inflammatory environment. *Biochem Biophys Res Commun* 356: 662–667, 2007.

49. **Rhen T, Cidlowski JA.** Antiinflammatory action of glucocorticoids–new mechanisms for old drugs. *N Engl J Med* 353: 1711–1723, 2005.

50. **Roberge C, Carpentier AC, Langlois MF, Baillargeon JP, Ardilouze JL, Maheux P, Gallo-Payet N.** Adrenocortical dysregulation as a major player in insulin resistance and onset of obesity. *Am J Physiol Endocrinol Metab* 293: E1465–E1478, 2007.

51. **Sakaue H, Ogawa W, Matsumoto M, Kuroda S, Takata M, Sugimoto T, Spiegelman BM, Kasuga M.** Posttranscriptional control of adipocyte differentiation through activation of phosphoinositide 3-kinase. *J Biol Chem* 273: 28945–28952, 1998.

52. **Sandeep TC, Andrew R, Homer NZ, Andrews RC, Smith K, Walker BR.** Increased in vivo regeneration of cortisol in adipose tissue in human obesity and effects of the 11beta- hydroxysteroid dehydrogenase type 1 inhibitor carbenoxolone. *Diabetes* 54: 872–879, 2005.

53. **Schaffler A, Scholmerich J, Buchler C.** Mechanisms of disease: adipocytokines and visceral adipose tissue–emerging role in intestinal and mesenteric diseases. *Nat Clin Pract Gastroenterol Hepatol* 2: 103–111, 2005.

54. **Seckl JR, Walker BR.** Minireview: 11beta-hydroxysteroid dehydrogenase type 1- a tissue-specific amplifier of glucocorticoid action. *Endocrinology* 142: 1371–1376, 2001.

55. **Smoak KA, Cidlowski JA.** Mechanisms of glucocorticoid receptor signaling during inflammation. *Mech Ageing Dev* 125: 697–706, 2004.

56. **Straub RH, Hense HW, Andus T, Scholmerich J, Riegger GA, Schunkert H.** Hormone replacement therapy and interrelation between serum interleukin-6 and body mass index in postmenopausal women: a population-based study. *J Clin Endocrinol Metab* 85: 1340–1344, 2000.

57. **Tchkonia T, Giorgadze N, Pirtskhalava T, Thomou T, DePonte M, Koo A, Forse RA, Chinnappan D, Martin-Ruiz C, von Zglinicki T, Kirkland JL.** Fat depot-specific characteristics are retained in strains derived from single human preadipocytes. *Diabetes* 55: 2571–2578, 2006.

58. **Tilg H, Moschen AR.** Adipocytokines: mediators linking adipose tissue, inflammation and immunity. *Nat Rev Immunol* 6: 772–783, 2006.

59. **Tontonoz P, Hu E, Graves RA, Budavari AI, Spiegelman BM.** mPPAR gamma 2: tissue-specific regulator of an adipocyte enhancer. *Genes Dev* 8: 1224–1234, 1994.

60. **Ulick S, Tedde R, Mantero F.** Pathogenesis of the type 2 variant of the syndrome of apparent mineralocorticoid excess. *J Clin Endocrinol Metab* 70: 200–206, 1990.

61. **Wake DJ, Rask E, Livingstone DE, Soderberg S, Olsson T, Walker BR.** Local and systemic impact of transcriptional up-regulation of 11beta-hydroxysteroid dehydrogenase type 1 in adipose tissue in human obesity. *J Clin Endocrinol Metab* 88: 3983–3988, 2003.

62. **Wamil M, Andrew R, Chapman KE, Street J, Morton NM, Seckl JR.** 7-oxysterols modulate glucocorticoid activity in adipocytes through competition for 11beta-hydroxysteroid dehydrogenase type. *Endocrinology* 149: 5909–5918, 2008.

63. **Weisberg SP, McCann D, Desai M, Rosenbaum M, Leibel RL, Ferrante AW Jr.** Obesity is associated with macrophage accumulation in adipose tissue. *J Clin Invest* 112: 1796–1808, 2003.

64. **Xing H, Northrop JP, Grove JR, Kilpatrick KE, Su JL, Ringold GM.** TNF alpha-mediated inhibition and reversal of adipocyte differentiation is accompanied by suppressed expression of PPARg without effects on Pref-1 expression. *Endocrinology* 138: 2776–2783, 1997.

65. **Xu H, Barnes GT, Yang Q, Tan G, Yang D, Chou CJ, Sole J, Nichols A, Ross JS, Tartaglia LA, Chen H.** Chronic inflammation in fat plays a crucial role in the development of obesity-related insulin resistance. *J Clin Invest* 112: 1821–1830, 2003.

66. **Yeager MP, Guyre PM, Munck AU.** Glucocorticoid regulation of the inflammatory response to injury. *Acta Anaesthesiol Scand* 48: 799–813, 2004.

67. **Zhang TY, Daynes RA.** Glucocorticoid conditioning of myeloid progenitors enhances TLR4 signaling via negative regulation of the phosphatidylinositol 3-kinase-Akt pathway. *J Immunol* 178: 2517–2526, 2007.

209

Corrigendum

Volume 298, May 2010

Ishii-Yonemoto T, Masuzaki H, Yasue S, Okada S, Kozuka C, Tanaka T, Noguchi M, Tomita T, Fujikura J, Yamamoto Y, Ebihara K, Hosoda K, Nakao K. Glucocorticoid reamplification within cells intensifies NF-κB and MAPK signaling and reinforces inflammation in activated preadipocytes. *Am J Physiol Endocrinol Metab* 298: E930-E940, 2010. First published September 23, 2009; doi:10.1152/ajpendo.00320.2009; http://ajpendo.physiology.org/cgi/content/full/298/5/E930.

Originally, blots in Figures 2, 3, 4, 5 and 6 were adjusted to show representative blots without demarcation. Revised Figures 2, 3, 4, 5, and 6 are now presented showing representative blots that are clearly separated. 11β-HSD1 activity analyses were performed by running the samples in triplicate under the same conditions as done previously. Independent experiments were performed to confirm the reproducibility of the results. These new figures appear online, linked directly to the article (http://ajpendo.physiology.org/cgi/content/full/ajpendo.00320.2009/DC2). The authors apologize for the previous errors, none of which have altered the conclusions reached in this study.

Relevant use of Klotho in FGF19 subfamily signaling system in vivo

Ken-ichi Tomiyama[a,b,1], Ryota Maeda[a,b,1], Itaru Urakawa[c], Yuji Yamazaki[c], Tomohiro Tanaka[a,b], Shinji Ito[a,b], Yoko Nabeshima[a,b], Tsutomu Tomita[d], Shinji Odori[d], Kiminori Hosoda[d], Kazuwa Nakao[d], Akihiro Imura[a,b], and Yo-ichi Nabeshima[a,b,2]

[a]Department of Pathology and Tumor Biology, Graduate School of Medicine, Kyoto University, Sakyo-Ku, Kyoto 606-8501, Japan; [c]Pharmaceutical Research Laboratories, Kyowa Hakko Kirin Company, Ltd., Takasaki, Gunma 370-1295, Japan; [b]Core Research for Evolutional Science and Technology, Japan Science and Technology Corporation, Kawaguchi-shi, Saitama 332-0012, Japan; and [d]Department of Medicine and Clinical Science, Graduate School of Medicine, Kyoto University, Sakyo-Ku, Kyoto 606-8501, Japan

α-Klotho (α-Kl) and its homolog, β-Klotho (β-Kl) are key regulators of mineral homeostasis and bile acid/cholesterol metabolism, respectively. FGF15/ humanFGF19, FGF21, and FGF23, members of the FGF19 subfamily, are believed to act as circulating metabolic regulators. Analyses of functional interactions between α- and β-Kl and FGF19 factors in wild-type, α-kl⁻/⁻, and β-kl⁻/⁻ mice revealed a comprehensive regulatory scheme of mineral homeostasis involving the mutually regulated positive/negative feedback actions of α-Kl, FGF23, and 1,25(OH)₂D and an analogous regulatory network composed of β-Kl, FGF15/humanFGF19, and bile acids that regulate bile acid/cholesterol metabolism. Contrary to in vitro data, β-Kl is not essential for FGF21 signaling in adipose tissues in vivo, because (*i*) FGF21 signals are transduced in the absence of β-Kl, (*ii*) FGF21 could not be precipitated by β-Kl, and (*iii*) essential phenotypes in Fgf21⁻/⁻ mice (decreased expressions of Hsl and Atgl in WAT) were not replicated in β-kl⁻/⁻ mice. These findings suggest the existence of Klotho-independent FGF21 signaling pathway(s) where undefined cofactors are involved. One-to-one functional interactions such as α-Klotho/ FGF23, β-Klotho/FGF15 (humanFGF19), and undefined cofactor/ FGF21 would result in tissue-specific signal transduction of the FGF19 subfamily.

bile acid | cholesterol | mineral homeostasis | Cyp genes | energy source

T he physiological roles of the Klotho family have remained puzzling since the original mutant mouse was developed (1). α-Kl deficiency in mice led to a characteristic phenotype resembling premature aging symptoms in human (1). Thereafter, we found that the overproduction of 1,25(OH)₂D and altered mineral-ion homeostasis are the major cause of these premature aging-like phenotypes observed in α-kl⁻/⁻ mice, because the lowering of 1,25(OH)₂D activity by dietary restriction (a regimen in which α-kl⁻/⁻ mice are fed a vitamin D–deficient diet) (2) is able to rescue the premature aging–like phenotypes and enable α-kl–deficient mice to survive normally without obvious abnormalities. Recently we have reported that α-Kl interacts with fibroblast growth factor 23 (FGF23) in kidney and plays an essential role in maintaining serum 1,25(OH)₂D levels by regulation of key active vitamin D–metabolizing enzymes, 1α-hydroxylase (Cyp27b1), and 24-hydroxylalse (Cyp24) (3). We also found that α-Kl binds to Na⁺,K⁺-ATPase in choroid plexus, parathyroid glands, and the distal convoluted tubules (DCT) of the kidney where extracellular calcium concentration is coordinately regulated (4). In these tissues, Na⁺,K⁺-ATPase activity is controlled in an α-Kl–dependent manner for transepithelial calcium transport in the choroid plexus and DCT, and for regulated PTH secretion in the parathyroid glands. By associating with both Na⁺,K⁺-ATPase and circulating FGF23, α-Kl plays a multifunctional role in α-Kl expressing tissues to regulate calcium and phosphate concentrations in vivo. This led to the concept that α-Kl is a regulator that integrates mineral homeostasis (5).

We next identified β-kl, which shares structural identity and characteristics with α-kl (6). β-Kl is predominantly expressed in the liver, pancreas, and adipose tissues (6) distinct from α-Kl expressing tissues (1, 2). To understand the biological role(s) of β-Kl, we generated a mouse line lacking β-kl (7). Although there were no gross abnormalities in the appearance of β-kl⁻/⁻ mice, these mice exhibited an altered metabolism of bile acids, a group of structurally diverse molecules that are primarily synthesized in the liver from cholesterol, promote absorption of dietary lipids in the intestine, and stimulate biliary excretion of cholesterol (8). The enterohepatic circulation of bile acids is regulated largely in hepatocytes where bile acid biosynthesis is regulated by rate-limiting enzymes; cholesterol 7α-hydroxylase (Cyp7a1) and sterol 12α-hydroxylase (Cyp8b1) (8). Bile acids and oxysterols act as ligands to nuclear receptors regulating the expression of important genes in cholesterol homeostasis (9). Particularly, bile acids bind to the promoter region of the farnesoid X receptor (FXR), which induces transcription of small heterodimer partner (SHP), a negative regulator of Cyp7a1 and Cyp8b1, resulting in suppression of bile acids synthesis in a negative feedback manner (9).

Simultaneously, Inagaki et al. reported that FGF15 dramatically suppresses expression of Cyp7a1 through a gut–liver signaling pathway that is different from the FXR/SHP-mediated negative feedback system (10). Moreover, the association of bile acids with FXR leads to the increase of Fgf15 expression in intestine, resulting in repression of Cyp7a1 in the liver. Importantly, this negative feedback effect was not observed in Fgf15⁻/⁻ and Fgfr4⁻/⁻ mice, and highlighted a concept that the binding of FGF15 with FGFR4 is involved in a second negative feedback system in bile acid metabolism. Taken together, analogous to the role of α-Kl in FGF23/FGFR1-mediated signal transduction, it was hypothesized that β-Kl plays a critical role in FGF15/FGFR4 mediated negative feedback regulation of Cyp7a1 and Cyp8b1 expression in the liver (11).

The mammalian FGF family currently consists of 22 members subdivided into seven subfamilies based on their structural similarity and modes of action (12). Most FGFs play an important role as paracrine factors regulating cell growth, regeneration, differentiation, and morphogenesis (13). However, it has been established that members of the FGF-19 subfamily, which also includes FGF21 and FGF23, differ in two important aspects from other FGF proteins. First, they have no or very small mitotic

---

effects; and second, they exert their action via systemic, hormone-like effects as metabolic regulators. In fact, human FGF19 (hFGF19) and its murine ortholog FGF15, as well as FGF23, are secreted from ileal enterocytes and bone, respectively, and then circulate in the bloodstream to target tissues (12–14). The third member, FGF21 is predominantly synthesized in the liver (15) and has beneficial effects on several metabolic parameters in different animal models of obesity; recently, FGF21 has been postulated to be a newly found regulator of glucose metabolism through induction of glucose transporter 1 (GLUT 1) (16).

As first shown for FGF23 and subsequently for FGF19, FGF21 has been predicted to require a specific cofactor for its binding to a certain type of FGFR and subsequent activation of FGF21/FGFR signaling pathway. β-Kl has been reported as a candidate cofactor essential for bioactivity of FGF21 in in vitro studies (16–22). However, these have not been confirmed in in vivo studies. It is particularly important to examine (i) whether FGF21 signal transduction is abolished in β-$kl^{-/-}$ mice and (ii) whether the phenotypes of β-$kl^{-/-}$ mice significantly overlap with those of $Fgf21$-deficient mice ($Fgf21^{-/-}$) (23, 24).

Recent advances in understanding the signaling of FGF19 subfamilies have mainly been based on conventional in vitro experiments (13, 17, 19, 22), whereas in vivo verification of the association of FGF ligands and FGF receptor or of FGF ligands and Klotho family proteins, as well as the signal transduction (phosphorylation) cascades triggered by FGF 19 subfamilies have yet to be confirmed.

In the present study, we demonstrate the first manifest evidence revealing that whereas α-Kl and β-Kl are required for FGF23 and FGF15/hFGF19-mediated signaling pathways in vivo, respectively, β-Kl appears not to be essential for FGF21-mediated signal transduction in vivo.

Results

α-Kl–Dependent Vitamin D Regulation by FGF23. FGF23 is derived from bone and is essential for maintaining phosphate homeostasis and regulation of vitamin D metabolism. In WT mice, administration of hFGF23 results in remarkable suppression of serum 1,25-dihydroxyvitamin D [1,25(OH)$_2$D] through the repression of $Cyp27b1$ and induction of $Cyp24$ in the kidney. As we previously reported, serum concentrations of 1,25(OH)$_2$D in both α-$kl^{-/-}$ and $Fgf23^{-/-}$ mice were remarkably higher than that of WT mice (2, 25). Intriguingly, serum FGF23 in α-$kl^{-/-}$ mice was >8,000-fold that of WT mice (Fig. 1A). To analyze how α-Kl and FGF23 coordinately regulate vitamin D metabolism in the kidney, we analyzed the interactive actions of FGF23 and α-Kl in vivo. The FGFs used in these experiments (hFGF23, hFGF19, hFGF21) were prepared from CHO cell culture media, and their activities were estimated by measuring Egr-1-promotor directed Luciferase activities using Peak rapid cells with or without exogenous expression of α-kl or β-kl (Fig. S1). Furthermore the activity of hFGF21 was confirmed by up-regulation of $Glut1$ mRNA in 3T3-L1 adipocyte. To minimize the effects of hypervitaminosis D, a major cause of the abnormalities observed in α-$kl^{-/-}$ mice, we used α-$kl^{-/-}$ mice fed with a vitamin D–deficient diet, in which serum 1,25(OH)$_2$D levels were normal and consequently most of the premature aging–like phenotypes were alleviated (2).

hFGF23 administration induced a significant decrease in serum 1,25(OH)$_2$D levels in WT mice, whereas no effect was observed in α-$kl^{-/-}$ mice (Fig. 1B). Consistently, in WT kidneys injected with hFGF23, $Cyp27b1$ expression was reduced >13-fold, whereas $Cyp24$ expression was induced >5-fold (Fig. 1 C and D). However, no significant effect of hFGF23 was found on the expression of $Cyp27b1$ and $Cyp24$ in α-$kl^{-/-}$ mice. These results offer direct evidence that α-Kl is essential for FGF23-derived repression of $Cyp27b1$ and induction of $Cyp24$ in vivo. In addition, we found that the administration of hFGF23 resulted in down-regulation of α-Kl expression (Fig. 1E), probably because α-Kl is a target of FGF23 signal trans-
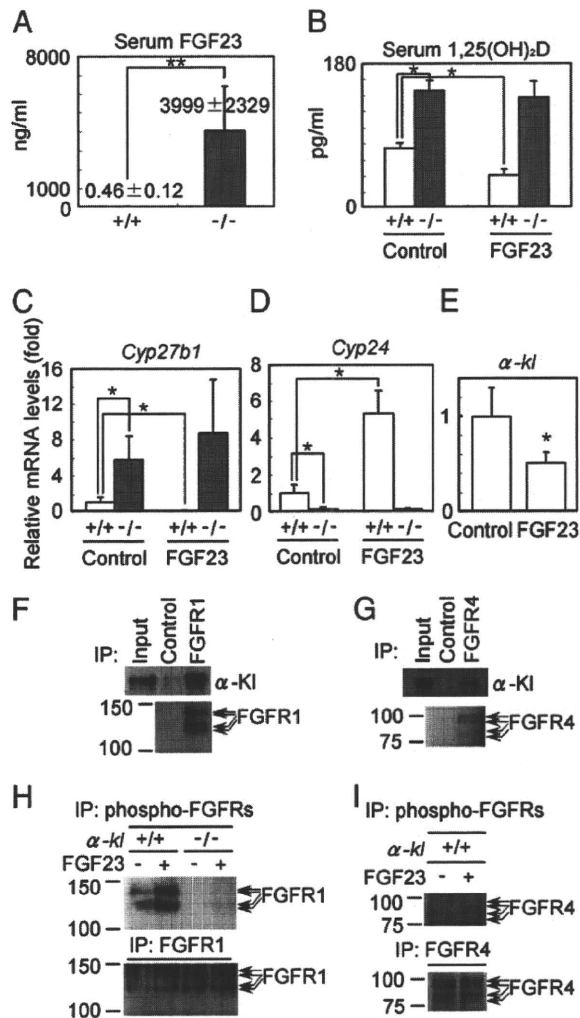

Fig. 1. FGF23 is dependent on α-Kl for regulation of vitamin D synthesis in kidney (A–E). (A) Serum concentrations of FGF23 in WT and α-$kl^{-/-}$ were measured by ELISA. WT (open bars) and α-$kl^{-/-}$ (filled bars) mice (n = 4/group) were injected with recombinant hFGF23 (0.2 mg/kg) or PBS control. Mice were killed 4 h after injection, and serum concentrations of 1,25(OH)$_2$D (B) were measured. $Cyp27b1$ (C), $Cyp24$ (D), and α-kl (E) mRNA levels in kidney were analyzed by RT–quantitative PCR. In this and all other figures, error bars represent mean ± SD and are plotted as fold change. Data were derived from 8- to 10-week-old male mice on vitamin D–deficient diets. *P < 0.05; **P < 0.01. FGFR1 binds to α-Kl and is phosphorylated by FGF23 in the kidney (F–I). (F) Kidney lysates were precipitated with anti-FGFR1 antibody or with control IgG. Input is 0.01% of the kidney whole extract used for the immunoprecipitation. (G) Kidney lysates were precipitated with anti-FGFR4 antibody or with control IgG. Input is 0.2% of the kidney whole extract used for the immunoprecipitation. (H) The kidney lysates of WT and α-$kl^{-/-}$ mice were immunoprecipitated with the anti-phospho-FGFRs or the anti-FGFR1 antibody. The immunoprecipitates were separated by SDS/PAGE and blotted with anti-FGFR1 antibody. (I) Kidney lysates of WT mice were immunoprecipitated with the anti-phospho-FGFRs or the anti-FGFR4 antibody and then blotted with anti-FGFR4 antibody.

duction and/or because of a secondary effect of decreased 1,25 (OH)$_2$D, an inducer of α-Kl gene expression (2). These data implicate an elaborate mutual negative feedback system composed of α-Kl, FGF23, and 1,25(OH)$_2$D in mineral-ion maintenance (Fig. 5A).

α-Kl–Dependent FGFR1 Phosphorylation by FGF23 in Vivo. Generally FGFs can bind to and activate cell surface tyrosine kinase FGF receptors and transduce signals to downstream molecules including MAP kinase (26). The FGF receptor family consists of

four members, FGFR1–4. With the exception of FGFR4, splicing variants in the third Ig-like domain (IIIb and IIIc types) have been identified for each member (12, 26). Recently, it has been reported that α-Kl binds to FGFRs in cultured cells (19) and converts the canonical FGFR1(III)c to a receptor specific for FGF23 (3). We therefore tested whether the above observations were valid in vivo. We first examined the interactions between α-Kl and FGFR1, and α-Kl and FGFR4 in the kidney. As observed in in vitro experiments, α-Kl was coprecipitated not only with FGFR1 but also with FGFR4 in the kidney (Fig. 1*F* and *G*). We then investigated whether these two receptors are activated by hFGF23 in the kidney (procedures are as in *SI Text* and Fig. S2). In WT mice, FGFR1 was activated in the kidney 10 min after injection of hFGF23 (Fig. 1*H*). In contrast, phosphorylation of FGFR4 was not detectable even after the injection of hFGF23 (Fig. 1*I*), suggesting that FGFR4 is not a major receptor responsible for FGF23 signaling in the kidney. As expected, we could not detect phosphorylation of FGFR1 in the kidney of α-$kl^{-/-}$ mice even after hFGF23 injection (Fig. 1*H*). In summary, we concluded that FGFR1 is preferentially activated by FGF23 in a α-Kl–dependent manner in the kidney.

β-Kl–Dependent Bile Acid Regulation by FGF15.

Because the unusually elevated expression of Cyp7a1 was observed not only in β-$kl^{-/-}$ mice (7) but also in $Fgf15^{-/-}$ and $Fgfr4^{-/-}$ mice (10, 27), we predicted that β-Kl was involved in FGF15/FGFR4-signaling system. Based on studies in cultured cells, it was recently proposed that β-Kl is necessary for FGF15/hFGF19-mediated signal transduction in the liver (18, 22). To confirm this hypothesis in vivo, we first measured the mRNA levels of *Fgf15* in the terminal ileum of WT and β-$kl^{-/-}$ mice. Interestingly, *Fgf15* expression levels were ~12-fold increased in β-$kl^{-/-}$ mice compared with those of WT (Fig. 2*A*), analogous to the elevation of FGF23 expression in α-$kl^{-/-}$ mice (Fig. 1*A*). To evaluate the effect of FGF15 in vivo, we administered hFGF19 and analyzed *Cyp7a1* and *Cyp8b1* expression. In WT mice, the expression levels of *Cyp7a1* and *Cyp8b1* 6 h after hFGF19 injection resulted in >100-fold and >10-fold reductions, respectively (Fig. 2 *B* and *C*). These were comparable to findings in a previous study examining FGF15 (10), and thus we concluded hFGF19 could be used to evaluate bile acid regulation in mice. In contrast, the expression levels of *Cyp7a1* and *Cyp8b1* remained elevated in β-$kl^{-/-}$ livers even after the administration of hFGF19 (Fig. 2 *B* and *C*), demonstrating that β-Kl is essential for the negative regulation of Cyp7a1 and Cyp8b1 by FGF15/hFGF19 in vivo. β-Kl-regulated bile acid synthesis by FGF15/hFGF19 is further described in *SI* (Fig. S3).

β-Kl/FGFR4 Coexpression Is Required for FGF15 Signaling in Vivo.

To monitor whether FGF15/hFGF19 signals are transduced in tissues other than the liver, we verified *Egr-1* (a zinc-finger transcription factor identified as an immediate-early gene induced by cellular stimulation) mRNA levels in β-Kl–expressing tissues (liver, adipose, pancreas, and salivary gland) as well as several β-Kl–nonexpressing tissues, since hFGF23 administration remarkably increased *Egr-1* expression and induced phosphorylation of 44/42 MAP kinase (ERK1/2) in the kidney where α-Kl is expressed (3). In WT liver, *Egr-1* expression level increased by >120-fold 30 min after hFGF19 administration compared with vehicle (Fig. 2*D*). With respect to other tissues, we observed a faint, but statistically significant *Egr-1* increase in pancreas (>5-fold) and in white adipose tissue (WAT) (~3-fold). Nonetheless, no remarkable changes were observed in other tissues including brown adipose tissue (BAT) and salivary gland despite β-Kl expression. As expected, in β-$kl^{-/-}$ mice injected with hFGF19, no significant induction of *Egr-1* was observed in any of the tissues evaluated (Fig. 2*D*), demonstrating that β-Kl is necessary but not sufficient for FGF15/hFGF19-mediated signal transduction. To address the question of why FGF15/hFGF19 signal is transduced in the liver, pancreas, and WAT, but not in BAT and
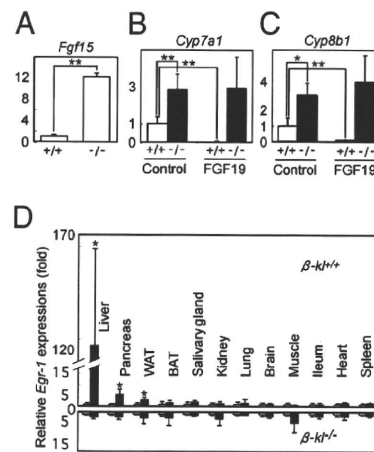
Fig. 2. FGF19 is dependent on β-Kl for regulation of bile acid synthesis in liver (*A–D*). (*A*) mRNA levels of *Fgf15* in terminal ileum in WT and β-$kl^{-/-}$ were measured by RTQ-PCR. WT mice (*open bars*) and β-$kl^{-/-}$ mice (*filled bars*) (*n* = 5/group) were injected with recombinant hFGF19 (1 mg/kg) or control medium. Mice were killed 6 h after injection and *Cyp7a1* (*B*) and *Cyp8b1* (*C*) mRNA levels in liver were measured by RT–quantitative PCR. Data were derived from 14- to 16-week-old male mice on standard diet. Egr-1 induction mediated by FGF19 in liver (*D*). hFGF19 (1 mg/kg) or control medium were injected into WT and β-$kl^{-/-}$ male mice (12–14 weeks old) on standard diet. Thirty minutes after injection, tissues in WT (*Upper*) and β-$kl^{-/-}$ (*Lower*) mice (*n* = 4/group) were excised. *Egr-1* mRNA levels were measured by RT-quantitative PCR. The expression levels of FGF19-injected mice (*filled bars*) and vehicle injected mice (*open bars*) are plotted as fold change. *P < 0.05; **P < 0.01.

salivary glands, we profiled the expression of various FGF receptors (FGFRs) in β-Kl–expressing tissues. As reported previously (10), FGFR4 is postulated to be the major receptor responsible for FGF15-mediated signal transduction in the liver. As for the pancreas and WAT, we did observe >2-fold and >6-fold lower *Fgfr4* expression compared with that in the liver, respectively. On the contrary, *Fgfr4* mRNA was not detected in the salivary glands and BAT (Fig. S4). Hence *Egr-1* up-regulation by hFGF19 could be observed in tissues where β-Kl and FGFR4 are coexpressed.

To further demonstrate the contribution of β-Kl in the hepatic FGF15/hFGF19-mediated signaling cascade, we evaluated the phosphorylation of FGFR4 and downstream signaling molecules in vivo using the methods shown in Fig. 1 (Fig. S2 and *SI Text*). β-Kl could be efficiently precipitated by an anti-FGFR4 antibody (Fig. 3*A*) and the phosphorylation of FGFR4 was confirmed after hFGF19 treatment in WT liver (Fig. 3*B*). Unexpectedly, the amount of FGFR4 protein was significantly reduced in livers of β-$kl^{-/-}$ mice (Fig. 3*C*). To obtain an amount of FGFR4 equivalent to that obtained from WT mice, we concentrated the liver lysates from β-$kl^{-/-}$ mice and performed immunoprecipitation (Fig. S2 and *SI Text*). However, we could not detect enhanced activation of FGFR4 in β-$kl^{-/-}$ livers even after injection of hFGF19 (Fig. 3*D*). Consistent with a previous report (18), clear phosphorylation of ERK1/2 was observed in WT livers 10 min after hFGF19 injection, whereas it was undetectable in β-$kl^{-/-}$ livers (Fig. 3*E*), demonstrating that β-Kl is essential for the FGF15/hFGF19 directed activation of FGFR4 and downstream signaling cascade in the liver.

β-Kl Is Not Essential for FGF21-Mediated Signaling in Adipose Tissues.

FGF21, a member of the FGF19 subfamily that is synthesized in the liver, has been reported to be a newly found regulator of glucose metabolism (16) and β-Kl has been postulated to be essential for its activity in in vitro studies (17, 20, 21). To examine the possible contribution of β-Kl in the FGF21 signaling system in vivo, we first administered recombinant hFGF21 to WT mice and analyzed *Egr-1* mRNA levels in multiple tissues (Fig. 4*A*). Before its use, we con-
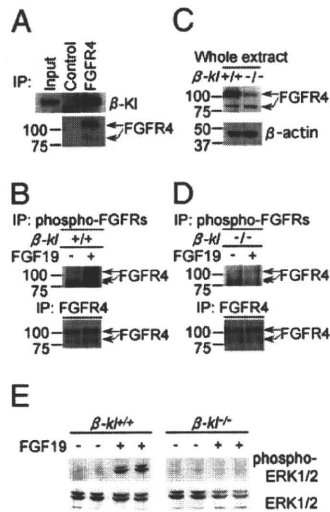
Tomiyama et al.

Fig. 3. FGFR4 binds to β-Kl and is phosphorylated by FGF19 in liver. (*A*) Liver lysates were precipitated with anti-FGFR4 antibody or with control IgG. Input is 1% of the liver whole extract used for the immunoprecipitation. The immunoprecipitates were separated by SDS/PAGE and blotted with anti-FGFR4 antibody. (*B*, *D*, and *E*) Ten minutes after injection of hFGF19 or control medium, livers were excised. Liver lysates from WT mice (*B*) and β-kl$^{-/-}$ mice (*D*) were immunoprecipitated with the anti–phospho-FGFRs or the polyclonal anti-FGFR4 antibody. Immunoprecipitates were blotted with anti-FGFR4 antibody. The arrowhead indicates a nonspecific band (Fig. S2). (*C*) Whole liver extracts of WT and β-kl$^{-/-}$ mice were blotted with anti-FGFR4 antibody or anti–β-actin antibody for a loading control. (*E*) Liver lysates from WT and β-kl$^{-/-}$ were immunoblotted with anti-phospho-ERK1/2 or anti-ERK1/2 antibodies (*n* = 2 in each case).

firmed the biological activity of the synthesized hFGF21. As shown in Fig. S5, our hFGF21 could enhance *Egr1*-derived luciferase reporter expression in a β-Kl–dependent manner at doses that were equivalent to those previously reported (17, 21). Moreover the hFGF21 up-regulated *Glut1* mRNA in 3T3-L1 adipocyte (Fig. S5) (16). Consistent with the in vitro results, in WT mice, *Egr-1* expression levels were significantly up-regulated by ~10-fold in WAT and >6-fold in BAT 30 min after injection of hFGF21 (Fig. 4*A* and Fig. S5). However, administration of hFGF21 also resulted in significant up-regulation of *Egr-1* mRNA levels in WAT and BAT from β-kl$^{-/-}$ mice (Fig. 4*B*). We next analyzed the serum levels of FGF21 and hepatic mRNA levels of *Fgf21* in WT and β-kl$^{-/-}$ mice. Unexpectedly, there was no significant genotype-dependent difference in mean serum protein concentrations of FGF21 nor hepatic *Fgf21* mRNA levels (Fig. 4 *C* and *D*). We also confirmed that β-kl expression was not affected by FGF21 administration (Fig. 4*E*). These results suggest that β-Kl is not essential for FGF21-mediated signaling in WAT and BAT. In addition, our prediction was further supported by the following experiments. First, to address the binding properties between β-Kl and FGF21, we performed pull-down assays using recombinant proteins. Although FGF19 was significantly bound by β-Kl in the presence of FGFR4, FGF21 could not be precipitated by β-Kl even with 10 fold amounts of FGF21 (Fig. 4 *F* and *G* and *SI Text*). Second, we compared the phenotypes of *Fgf21*$^{-/-}$ and β-kl$^{-/-}$ mice. Recently, Hotta et al. developed *Fgf21*$^{-/-}$ mice and reported that expression levels of hormone-sensitive lipase (*Hsl*) and adipose triglyceride lipase (*Atgl*) in WAT were decreased in *Fgf21*$^{-/-}$ mice to almost 50% compared with those of WT mice (23). The adipose phenotypes in *Fgf21*$^{-/-}$ mice may be an outcome of a deficiency in FGF21 signaling. Thus we analyzed the expression levels of these genes in the adipose tissues of β-kl$^{-/-}$ mice. Consequently, in both WAT and BAT, mRNA levels of *Hsl* and *Atgl* were not significantly altered between WT and β-kl$^{-/-}$ mice (Fig. 4 *H* and *I*). These data suggest that β-Kl may not necessarily be involved in the phenotypes observed in FGF21-
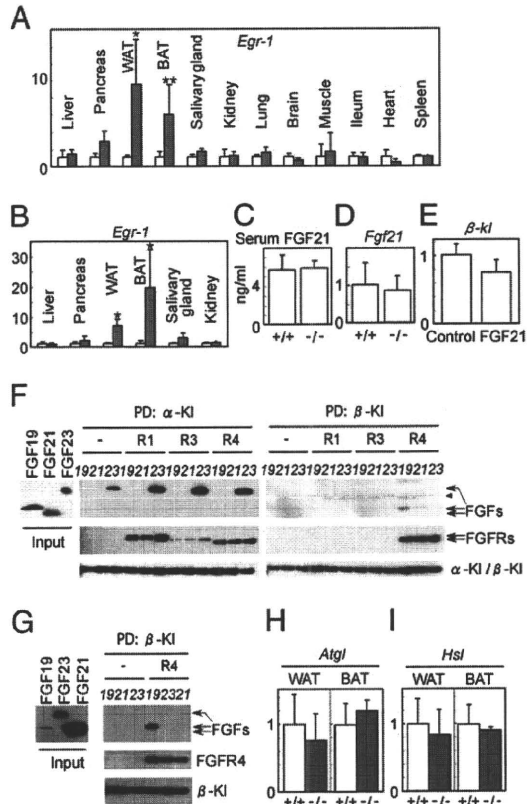

Fig. 4. β-Kl is not essential for FGF21-mediated signaling (*A*–*I*). Thirty minutes after injection, tissues in WT (*n* = 5/group) (*A*) and β-kl$^{-/-}$ mice (*n* = 4/group) (*B*) were excised. *Egr-1* mRNA levels were measured by RT-quantitative PCR. The expression levels of hFGF21 injected mice (*filled bars*) and vehicle injected mice (*open bars*) mice are plotted as fold change. Data were derived from 7- to 10-week-old male mice on standard diet. (*C*) Serum FGF21 concentrations of WT and β-kl$^{-/-}$ mice (*n* = 5–6/group) were measured by RIA. (*D*) *Fgf21* mRNA levels in livers of WT and β-kl$^{-/-}$ mice (*n* = 5–6/group) were measured by RT-quantitative PCR and are plotted as fold change. Data were derived from 15- to 20-week-old male mice on standard diet. hFGF21 (0.4 mg/kg) or control medium were injected into WT and β-kl$^{-/-}$ mice. (*E*) WT mice were injected with recombinant hFGF21 (0.4 mg/kg) or control medium (*n* = 5/group). Mice were killed 4 h after injection and β-kl mRNA levels in WAT were analyzed by RT-quantitative PCR. Data were derived from 10-week-old male mice on standard diet. (*F*) A 15-ng quantity of each FGF was pulled down (PD) by α-/β-Kl in the presence (R1, R3, or R4) or absence (–) of FGFRs. Input was 8% of samples used for the pull-down assay. Samples of pulled down by α-/β-Kl were analyzed by SDS/PAGE and blotted with antibodies (anti-His for FGFs, anti-Human Fc for FGFRs, and anti-GFP for α-/β-Kl). Arrowhead indicates a nonspecific band. (*G*) A 50-ng quantity of FGF19, 150 ng of FGF23, or 500 ng of FGF21 was precipitated by β-Kl in the presence or absence of FGFR4. Input was 1% of samples used for the assay. (*H* and *I*) *hsl* and *atgl* mRNA levels in WAT and BAT were analyzed by RT-quantitative PCR. Data were derived from 9- to 14-week-old female β-kl$^{+/+}$ and β-kl$^{-/-}$ mice (*n* = 5/group). *$P < 0.05$; **$P < 0.01$.

deficient mice. Taken together, these results provide strong evidence that β-Kl is not essential for FGF21-mediated signaling in WAT and BAT. We therefore asked whether FGF21 signaling might require other unidentified components than β-Kl. We also analyzed *Glut1* mRNA levels 4 h after hFGF21 injection at concentrations that could induce *Egr-1* expression in WAT and BAT, but no apparent induction was observed, suggesting that *Glut1* is not a direct target of FGF21 signaling (28, 29).

Discussion

Various roles of Klotho family members have been reported (18, 22, 30); however, a consensus on the molecular functions of α-Kl

and β-Kl has not been reached. Based on these findings, we propose a comprehensive regulatory scheme of mineral homeostasis that is illustrated by the mutually regulated positive/negative feedback actions of α-Kl, FGF23, and 1,25(OH)₂D (Fig. 5A). In the present study, we found that FGF23 represses the expression of α-Kl and identified an essential role of α-Kl in FGF23-mediated phosphorylation of FGFR1 in the kidney. This leads to *Cyp27b1* downregulation and *Cyp24* up-regulation, and results in inhibition of the synthesis of 1,25(OH)₂D, an active form of vitamin D (3). 1,25 (OH)₂D has prominent effects on the kidney, intestine, and bone. In the kidney, 1,25(OH)₂D activates vitamin D receptor (VDR) by binding to its ligand binding domain and negatively regulates the expression of *Cyp27b1* while positively regulating *Cyp24* and α-Kl expression (2). In the bone, 1,25(OH)₂D binds to VDR and induces FGF23 synthesis in osteocytes and osteoblasts (31) in hours/days. In turn, secreted FGF23 suppresses 1,25(OH)₂D synthesis and inorganic phosphate reabsorption in the kidney to adjust extracellular mineral concentrations. Collectively, α-Kl, in combination with FGF23, is involved in a signaling cascade that maintains extracellular calcium/phosphate levels within a narrow range.

The roles of β-Kl, FGF15, and FGFR4 in bile acid/cholesterol metabolism are schematically summarized in Fig. 5B. Consistent with a previous study (10, 22), i.v. injection of hFGF19 dramatically represses the expression of *Cyp7a1* and *Cyp8b1* and results in the inhibition of bile acid synthesis from cholesterol in WT livers. This suppression of *Cyp7a1* and *Cyp8b1* was not observed in *β-kl⁻/⁻* mice. Indeed, phosphorylation of FGFR4 and ERK1/2 was not detected in *β-kl⁻/⁻* livers even after hFGF19 administration. Our findings provide conclusive evidence proving the essential role of β-Kl in FGF15/hFGF19-mediated activation of FGFR4 and subsequent signal transduction that regulates bile acid synthesis. Particularly, by binding to FXR, bile acid induces SHP expression in the liver and FGF15 transcription in the terminal ileum. In turn, increased SHP and secreted FGF15 differentially suppress Cyp7a1/Cyp8b1 expression to downregulate bile acid synthesis (8, 9, 11). In addition, we found mutual negative feedback regulations between β-Kl and FGF15, namely, a decrease in *β-kl* after hFGF19 administration and an increase in *Fgf15* in *β-kl* deficiency. In other words, *β-kl* ablation leads to impaired negative feedback regulation of bile acid metabolism, resulting in the overflow of bile acid pools. Consequently, in the *β-kl⁻/⁻* terminal ileum, chronic stimulation by elevated bile acid would lead to an unusual increase in *Fgf15* mRNA. We propose a scheme illustrating the bile acid/cholesterol homeostasis regulated by mutual negative/positive feedback actions of β-Kl, FGF15, and bile acids (Fig. 5B).

As shown in Fig. 5, the scheme for bile acid regulation by β-Kl/FGF15 is conceptually analogous to that of vitamin D metabolism, which involves α-Kl and FGF23. Both systems are regulated by the

coordination of two types of feedback mechanisms mediated by end-metabolites, 1,25(OH)₂D or bile acids, that are in situ negative feedback regulation and target tissue mediated negative feedback loop. In the former pathway, the end-metabolite functions as a nuclear receptor ligand and negatively feeds back by repressing the expression of key regulatory enzymes (Cyp27b1 in the kidney or Cyp7a1/Cyp8b1 in the liver) in the relevant metabolic pathway responsible for the generation of end-metabolite itself. In the latter system, the end-metabolite is transported to the target tissue (bone or intestine) from a distal site and enhances the expression of FGF (FGF23 or FGF15) by binding to the nuclear receptor; VDR or FXR. Subsequently, secreted FGF acts as the regulator of a target tissue–mediated negative feedback loop in collaboration with α-Kl or β-Kl. The next question to be addressed is how these two pathways are coordinately involved in the rapid adjustment and long term maintenance of mineral homeostasis and bile acid metabolism.

In a previous report, we showed that i.v. injection of hFGF23 induces phosphorylation of ERK1/2 and specifically up-regulates the expression of *Egr-1* in the murine kidney (3). Here we demonstrate that α-Kl is required for FGF23 signal transduction in vivo. Likewise, i.v. injection of hFGF19 results in ERK1/2 phosphorylation and up-regulation of *Egr-1* in the liver in a β-Kl–dependent manner. Among β-Kl–expressing organs, significant up-regulation of *Egr-1* was observed in tissues where β-Kl and FGFR4 are coexpressed. Although induction of *Egr-1* in pancreas and WAT are slight, it occurs in a β-Kl–dependent manner. FGF15-mediated signal in pancreas and WAT could therefore be involved in bile acid homeostasis, but its functional importance has yet to be elucidated. Furthermore, the very high *Egr-1* induction in the liver strongly suggests that other elements, in addition to the coexpression of β-Kl and FGFR4, may endow this prominent hepatic signal activation. Recently, several groups have reported that α-Kl and β-Kl can bind to certain types of FGFRs. Those studies report preferences and differences for this binding that might be dependent on assay conditions. α-Kl solely binds to FGFR1(IIIc) in vitro (3), however α-Kl binds to not only FGFR1(IIIc) but also FGFR4 and weakly to FGFR3(IIIc) in cultured cells (30). Even though FGFR4 could precipitate α-Kl in the kidney, activation of FGFR4 by hFGF23 could not be detected. Further studies are required to understand how FGFR(s) is definitively and preferentially used for a particular FGF signal in vivo.

Serum levels of FGF23 and ileac *Fgf15* mRNA expression were intensively increased in *α-kl⁻/⁻* and *β-kl⁻/⁻* mice, respectively. Furthermore, administrations of hFGF23 and hFGF19 apparently suppressed the expression of *α-kl* and *β-kl*, respectively. In contrast, the serum levels of FGF21 and hepatic *Fgf21* mRNA expression were not increased in *β-kl⁻/⁻* mice, and *β-kl* expression was not significantly suppressed by hFGF21 in adipose. Consistent with a previous report that FGF21 induces ERK1/2 phosphorylation specifically in WAT (17), administration of FGF21 to WT mice significantly induced *Egr-1* mRNA expression in WAT and BAT, suggesting that WAT and BAT were the possible target tissues of FGF21. However, surprisingly, remarkable *Egr-1* inductions in WAT and BAT were also observed in *β-kl⁻/⁻* mice, indicating that β-Kl is not essential for FGF21 signal transduction in vivo. These in vivo results contrasted with those obtained from in vitro assays, as β-Kl is essential for FGF21-mediated signal transduction in vitro. We reproduced the direct binding of α-Kl and hFGF23 and also confirmed tricomplex formation of β-Kl, hFGF19, and FGFR4 but were unable to detect binding of α-/β-Kl and hFGF21 in our pull-down assay (Fig. 4G). Furthermore, we confirmed that the adipose phenotypes in *Fgf21⁻/⁻* mice did not overlap with those of *β-kl⁻/⁻* mice. This inconsistency leads to a postulation that β-Kl is not necessary for FGF21 signaling.

Currently, β-Kl is believed to be a common player essential for FGF15- and FGF21-mediated signal transduction. However, our present results, together with the data from Hotta et al. (23), do
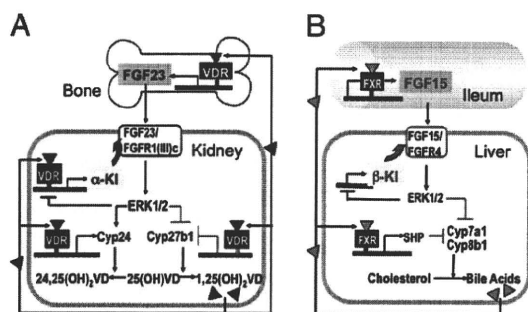

Fig. 5. Schematic representation of α-Kl/FGF23 and β-Kl/FGF15 systems. (A) Regulatory network of mineral homeostasis illustrated by the mutual positive/negative feedback actions of α-Kl, FGF23, and 1,25(OH)₂D. (B) Regulatory network of bile acid/cholesterol metabolism represented by the mutual positive/negative feedback actions of β-Kl, FGF15, and bile acids.

215

not support this hypothesis. Possible explanations are that the response found in cultured cells might be caused by: (*i*) an artificial abundance of β-Kl and/or FGF21, (*ii*) peculiar characteristics of the cultured cells used in these experiments, and/or (*iii*) a combination of these two factors (17, 20, 21).

Recent studies have reported that FGF21 stimulates lipolysis in WAT and ketogenesis in the liver (32, 33). However, those results represent the pharmacological effects of sustained FGF21 treatment and thus include consequences that are secondary and indirectly induced by FGF21. We propose a β-Kl–independent response directly triggered by hFGF21 administration. Significant *Egr-1* upregulation in WAT and BAT are indicative that FGF21 mediates lipid metabolism in adipose tissues. The physiological target(s) of FGF21 signaling need to be clarified to understand how FGF21 functions as a regulator of lipid metabolism. Observations using genetic manipulation will lead us to a precise understanding of the roles of the FGF19 subfamily in metabolic homeostasis in vivo.

Materials and Methods

Measurement of Serum Parameters. Blood samples were collected from orbital cavities or hearts under anesthesia and were centrifuged to obtain sera. Serum FGF23 levels were measured by sandwich ELISA (Kainos Laboratory), which can quantify the intact form or FGF23 using human recombinant FGF23 as a standard. Serum $1,25(OH)_2D$ levels were analyzed by SRL, Inc. Serum FGF21 levels were measured by specific RIA (Phoenix Pharmaceuticals, Inc.).

Statistical Analysis. Unless otherwise noted, all values are expressed as mean ± SD. All data were analyzed by the Mann–Whitney *U* test. *P* values less than 0.05 were considered to be statistically significant.

More details are described in *SI Materials and Methods*.

1. Kuro-o M, et al. (1997) Mutation of the mouse Klotho gene leads to a syndrome resembling ageing. *Nature* 390:45–51.
2. Tsujikawa H, Kurotaki Y, Fujimori T, Fukuda K, Nabeshima Y (2003) Klotho, a gene related to a syndrome resembling human premature aging, functions in a negative regulatory circuit of vitamin D endocrine system. *Mol Endocrinol* 17:2393–2403.
3. Urakawa I, et al. (2006) Klotho converts canonical FGF receptor into a specific receptor for FGF23. *Nature* 444:770–774.
4. Imura A, et al. (2007) alpha-Klotho as a regulator of calcium homeostasis. *Science* 316: 1615–1618.
5. Nabeshima Y, Imura H (2008) alpha-Klotho: A regulator that integrates calcium homeostasis. *Am J Nephrol* 28:455–464.
6. Ito S, et al. (2000) Molecular cloning and expression analyses of mouse betaklotho, which encodes a novel Klotho family protein. *Mech Dev* 98:115–119.
7. Ito S, et al. (2005) Impaired negative feedback suppression of bile acid synthesis in mice lacking betaKlotho. *J Clin Invest* 115:2202–2208.
8. Russell DW (2003) The enzymes, regulation, and genetics of bile acid synthesis. *Annu Rev Biochem* 72:137–174.
9. Goodwin B, et al. (2000) A regulatory cascade of the nuclear receptors FXR, SHP-1, and LRH-1 represses bile acid biosynthesis. *Mol Cell* 6:517–526.
10. Inagaki T, et al. (2005) Fibroblast growth factor 15 functions as an enterohepatic signal to regulate bile acid homeostasis. *Cell Metab* 2:217–225.
11. Jones S (2008) Mini-review: Endocrine actions of fibroblast growth factor 19. *Mol Pharm* 5:42–48.
12. Itoh N, Ornitz DM (2004) Evolution of the Fgf and Fgfr gene families. *Trends Genet* 20:563–569.
13. Itoh N, Ornitz DM (2008) Functional evolutionary history of the mouse Fgf gene family. *Dev Dyn* 237:18–27.
14. Nishimura T, Utsunomiya Y, Hoshikawa M, Ohuchi H, Itoh N (1999) Structure and expression of a novel human FGF, FGF-19, expressed in the fetal brain. *Biochim Biophys Acta* 1444:148–151.
15. Nishimura T, Nakatake Y, Konishi M, Itoh N (2000) Identification of a novel FGF, FGF-21, preferentially expressed in the liver. *Biochim Biophys Acta* 1492:203–206.
16. Kharitonenkov A, et al. (2005) FGF-21 as a novel metabolic regulator. *J Clin Invest* 115: 1627–1635.
17. Ogawa Y, et al. (2007) BetaKlotho is required for metabolic activity of fibroblast growth factor 21. *Proc Natl Acad Sci USA* 104:7432–7437.
18. Kurosu H, et al. (2007) Tissue-specific expression of betaKlotho and fibroblast growth factor (FGF) receptor isoforms determines metabolic activity of FGF19 and FGF21. *J Biol Chem* 282:26687–26695.

19. Wu X, et al. (2007) Co-receptor requirements for fibroblast growth factor-19 signaling. *J Biol Chem* 282:29069–29072.
20. Suzuki M, et al. (2008) betaKlotho is required for fibroblast growth factor (FGF) 21 signaling through FGF receptor (FGFR) 1c and FGFR3c. *Mol Endocrinol* 22:1006–1014.
21. Kharitonenkov A, et al. (2008) FGF-21/FGF-21 receptor interaction and activation is determined by betaKlotho. *J Cell Physiol* 215:1–7.
22. Lin BC, Wang M, Blackmore C, Desnoyers LR (2007) Liver-specific activities of FGF19 require Klotho beta. *J Biol Chem* 282:27277–27284.
23. Hotta Y, et al. (2009) Fibroblast growth factor 21 regulates lipolysis in white adipose tissue but is not required for ketogenesis and triglyceride clearance in liver. *Endocrinology* 150:4625–4633.
24. Potthoff MJ, et al. (2009) FGF21 induces PGC-1alpha and regulates carbohydrate and fatty acid metabolism during the adaptive starvation response. *Proc Natl Acad Sci USA* 106:10853–10858.
25. Shimada T, et al. (2004) Targeted ablation of Fgf23 demonstrates an essential physiological role of FGF23 in phosphate and vitamin D metabolism. *J Clin Invest* 113: 561–568.
26. Powers CJ, McLeskey SW, Wellstein A (2000) Fibroblast growth factors, their receptors and signaling. *Endocr Relat Cancer* 7:165–197.
27. Yu C, et al. (2000) Elevated cholesterol metabolism and bile acid synthesis in mice lacking membrane tyrosine kinase receptor FGFR4. *J Biol Chem* 275:15482–15489.
28. Berglund ED, et al. (2009) Fibroblast growth factor 21 controls glycemia via regulation of hepatic glucose flux and insulin sensitivity. *Endocrinology* 150:4084–4093.
29. Xu J, et al. (2009) Fibroblast growth factor 21 reverses hepatic steatosis, increases energy expenditure, and improves insulin sensitivity in diet-induced obese mice. *Diabetes* 58:250–259.
30. Kurosu H, et al. (2006) Regulation of fibroblast growth factor-23 signaling by klotho. *J Biol Chem* 281:6120–6123.
31. Kolek OI, et al. (2005) 1alpha,25-Dihydroxyvitamin D3 upregulates FGF23 gene expression in bone: The final link in a renal-gastrointestinal-skeletal axis that controls phosphate transport. *Am J Physiol Gastrointest Liver Physiol* 289:G1036–G1042.
32. Inagaki T, et al. (2007) Endocrine regulation of the fasting response by PPARalpha-mediated induction of fibroblast growth factor 21. *Cell Metab* 5:415–425.
33. Badman MK, et al. (2007) Hepatic fibroblast growth factor 21 is regulated by PPARalpha and is a key mediator of hepatic lipid metabolism in ketotic states. *Cell Metab* 5:426–437.

PHYSIOLOGY

216

A Mutation in the Gene Encoding Mitochondrial Mg^{2+} Channel MRS2 Results in Demyelination in the Rat

Takashi Kuramoto[1]*, Mitsuru Kuwamura[2], Satoko Tokuda[1,2], Takeshi Izawa[2], Yoshifumi Nakane[1], Kazuhiro Kitada[1,3], Masaharu Akao[4], Jean-Louis Guénet[5], Tadao Serikawa[1]

1 Institute of Laboratory Animals, Graduate School of Medicine, Kyoto University, Kyoto, Japan, 2 Laboratory of Veterinary Pathology, Osaka Prefecture University, Osaka, Japan, 3 Laboratory of Mammalian Genetics, Genome Dynamics Research Center, Graduate School of Science, Hokkaido University, Sapporo, Japan, 4 Department of Cardiovascular Medicine, Graduate School of Medicine, Kyoto University, Kyoto, Japan, 5 Département de Biologie du Développement, Institut Pasteur, Paris, France

Abstract

The rat demyelination (*dmy*) mutation serves as a unique model system to investigate the maintenance of myelin, because it provokes severe myelin breakdown in the central nervous system (CNS) after normal postnatal completion of myelination. Here, we report the molecular characterization of this mutation and discuss the possible pathomechanisms underlying demyelination. By positional cloning, we found that a G-to-A transition, 177 bp downstream of exon 3 of the *Mrs2* (MRS2 magnesium homeostasis factor (*Saccharomyces cerevisiae*)) gene, generated a novel splice acceptor site which resulted in functional inactivation of the mutant allele. Transgenic rescue with wild-type *Mrs2*-cDNA validated our findings. *Mrs2* encodes an essential component of the major Mg^{2+} influx system in mitochondria of yeast as well as human cells. We showed that the *dmy/dmy* rats have major mitochondrial deficits with a markedly elevated lactic acid concentration in the cerebrospinal fluid, a 60% reduction in ATP, and increased numbers of mitochondria in the swollen cytoplasm of oligodendrocytes. MRS2-GFP recombinant BAC transgenic rats showed that MRS2 was dominantly expressed in neurons rather than oligodendrocytes and was ultrastructurally observed in the inner membrane of mitochondria. Our observations led to the conclusion that *dmy/dmy* rats suffer from a mitochondrial disease and that the maintenance of myelin has a different mechanism from its initial production. They also established that Mg^{2+} homeostasis in CNS mitochondria is essential for the maintenance of myelin.

Introduction

Myelin is an essential component of the nervous tissue of higher vertebrates. It acts as a natural insulator of axonal segments allowing, at the same time, the maintenance of axonal integrity and the fast conduction of action potentials. It also reduces ionic currents across the axonal membrane and stabilizes the extracellular milieu within rapidly-firing axon bundles.

In the central nervous system (CNS), myelin is produced by oligodendrocytes, while in the peripheral nervous system (PNS), this function is achieved by Schwann cells. Myelination is completed within a relatively short period of time during mammalian development and requires a high rate of production and transport of different kinds of molecules, mostly proteins and lipids. In adult life, myelin is constantly remodeled and the maintenance of functional myelin sheaths requires a careful balance of *de novo* synthesis and turnover. It is quite clear that any event generating an imbalance in the myelination or remyelination process has the greatest chance of inducing dys- or demyelination of either the central or peripheral nervous system.

Our knowledge of the myelination process has benefited from careful observations conducted on human patients affected by one of the many defects of myelination or myelin turnover. It has also benefited from researches carried out on animal models, mostly mutant mice and rats, including those that have been induced by transgenesis or genetic engineering in ES cell lines [1,2]. Some of these models have even allowed therapies to be developed in a preclinical setting [3]. Unfortunately, only a small number of the many genes that are directly or indirectly involved in the myelination process have been identified and only a few of these genes have been functionally annotated, for example, by the characterization of one or more mutant alleles. For this reason, any new mutation occurring spontaneously or after mutagenesis is of potential interest for unraveling the molecular mechanisms involved in myelin assembly.

In an earlier paper we reported the discovery and pathology of a rat mutation designated *demyelination* (symbol *dmy*), which is characterized by severe and progressive myelin breakdown in the CNS. We mapped the locus responsible for this myelin disorder to rat chromosome (Chr) 17, very close to the prolactin (*Prl*) locus, in a region homologous to human Chr 6p21.1-22.3 and mouse Chr 13 [4,5]. Based on its pathological features, as well as its genetic localization, this demyelination syndrome appeared to be unique, with no homologue so far reported in any other mammalian species, including humans.